Seasonal Variation of Oxygenated Organic Molecules in Urban Beijing and their Contribution to Secondary Organic Aerosol

Yishuo Guo[1], Chao Yan[1,2,3*], Yuliang Liu[2], Xiaohui Qiao[4], Feixue Zheng[1], Ying Zhang[1], Ying Zhou[1], Chang Li[1], Xiaolong Fan[1], Zhuohui Lin[1], Zemin Feng[1], Yusheng Zhang[1], Penggang Zheng[5,6], Linhui Tian[7], Wei Nie[2], Zhe Wang[5], Dandan Huang[8], Kaspar R. Daellenbach[3,9], Lei Yao[1,3], Lubna Dada[3,9], Federico Bianchi[3], Jingkun Jiang[4], Yongchun Liu[1], Veli-Matti Kerminen[3], Markku Kulmala[1,3]

Affiliations:

[1] Aerosol and Haze Laboratory, Beijing Advanced Innovation Center for Soft Matter Science and Engineering, Beijing University of Chemical Technology, Beijing, China

[2] Joint International Research Laboratory of Atmospheric and Earth System Research, School of Atmospheric Sciences, Nanjing University, Nanjing, China

[3] Institute for Atmospheric and Earth System Research / Physics, Faculty of Science, University of Helsinki, Finland

[4] State Key Joint Laboratory of Environment Simulation and Pollution Control, State Environmental Protection Key Laboratory of Sources and Control of Air Pollution Complex, School of Environment, Tsinghua University, Beijing, China

[5] Division of Environment and Sustainability, The Hong Kong University of Science and Technology, Hong Kong SAR, China

[6] Department of Civil and Environmental Engineering, The Hong Kong Polytechnic University, Hong Kong SAR

[7] Department of Civil and Environmental Engineering, Faculty of Science and Technology, University of Macau, Taipa, Macau, China

[8] State Environmental Protection Key Laboratory of Formation and Prevention of Urban Air Pollution Complex, Shanghai Academy of Environmental Sciences, Shanghai, China

[9] Laboratory of Atmospheric Chemistry, Paul Scherrer Institute, Villigen, Switzerland.

Correspondence to: Chao Yan (chaoyan@nju.edu.cn)

Abstract Oxygenated organic molecules (OOMs) are crucial for atmospheric new particle formation and secondary organic aerosol (SOA) growth. Therefore, understanding their chemical composition, temporal behavior, and sources is of great importance. Previous studies on OOMs mainly focus on environments where biogenic sources are predominant, yet studies on sites with dominant anthropogenic emissions, such as megacities, have been lacking. Here, we conducted long-term measurements of OOMs covering four seasons of the year 2019 in urban Beijing. The OOM concentration was found to be the highest in summer (1.6×10^8 cm^{-3}), followed by autumn (7.9×10^7 cm^{-3}), spring (5.7×10^7 cm^{-3}) and winter (2.3×10^7 cm^{-3}), suggesting that enhanced photo-oxidation together with the rise of temperature promote the formation of OOMs. Most OOMs contained 5 to 10 carbon atoms and 3 to 7 effective oxygen atoms ($nO_{eff} = nO - 2 \times nN$). The average nO_{eff} increased with increasing atmospheric photo-oxidation capacity, which was the highest in summer and the lowest in winter and autumn. By performing a newly developed workflow, OOMs were classified into four types: aromatic OOMs, aliphatic OOMs, isoprene OOMs, and monoterpene OOMs. Among them, aromatic OOMs (29-41 %) and aliphatic OOMs (26-41 %) were the main contributors in all seasons, indicating that OOMs in Beijing were dominated by anthropogenic sources. The contribution of isoprene OOMs increased significantly in summer (33 %), which is much higher than those in other three seasons (8-10 %).

38   Concentrations of isoprene ($0.2\text{-}5.3\times10^7$ cm^{-3}) and monoterpene ($1.1\text{-}8.4\times10^6$ cm^{-3}) OOMs in Beijing were lower

39   than those reported at other sites, and they possessed lower oxygen and higher nitrogen contents due to high NO$_x$

40   levels (9.5-38.3 ppbv) in Beijing. With regard to the nitrogen content of the two anthropogenic OOMs, aromatic

41   OOMs were mainly composed of CHO and CHON species, while aliphatic OOMs were dominated by CHON and

42   CHON$_2$ ones. Such prominent differences suggest varying formation pathways between these two OOMs. By

43   combining the measurements and an aerosol dynamic model, we estimated that the SOA growth rate through OOM

44   condensation could reach 0.64 μg·m^{-3}·h^{-1}, 0.61 μg·m^{-3}·h^{-1}, 0.41 μg·m^{-3}·h^{-1}, and 0.30 μg·m^{-3}·h^{-1} in autumn, summer,

45   spring, and winter, respectively. Despite the similar concentrations of aromatic and aliphatic OOMs, the former had

46   lower volatilities and, therefore, showed higher contributions (46-62%) to SOA than the latter (14-32%). By contrast,

47   monoterpene OOMs and isoprene OOMs, limited by low abundances or high volatilities, had low contributions of

48   8-12% and 3-5%, respectively. Overall, our results improve the understanding of the concentration, chemical

49   composition, seasonal variation and potential atmospheric impacts of OOMs, which can help formulate refined

50   restriction policy specific to SOA control in urban areas.

51

1. INTRODUCTION

Atmospheric aerosols affect global climate both directly and indirectly (Stocker, 2014) and are known to have a detrimental influence on human health (Lelieveld et al., 2015). Modeling studies have suggested that new particle formation (NPF) dominates the number concentration of particles and is an important contributor to cloud condensation nuclei (CCN) in the global atmosphere (Merikanto et al., 2009;Gordon et al., 2017). In terms of aerosol mass, it has been shown that a significant fraction is composed of secondary organic aerosol (SOA) (Zhang et al., 2007;Jimenez et al., 2009;Hallquist et al., 2009). In both NPF and SOA formation processes, oxygenated organic molecules (OOMs, see the definition in Sect. S2 the work of Nie et al. (Nie et al., 2022)) have been acknowledged as an important contributor, and thus advanced understanding of OOMs is crucial.

The role of OOMs in NPF was first suggested in 2002, but they could not be identified or quantified at that time (O'Dowd et al., 2002). Then, the emergence of Atmospheric Pressure interface Time-of-Flight (APi-ToF) mass spectrometer (Junninen et al., 2010;Ehn et al., 2010;Ehn et al., 2012) and Chemical Ionization-APi-ToF (CI-APi-ToF) mass spectrometer (Jokinen et al., 2012;Ehn et al., 2014) provided the first direct measurement of highly oxygenated organic molecules (HOMs), a subgroup of OOMs with the most oxygen content, which inspired later studies on their role in NPF and SOA growth (Kulmala et al., 2013;Schobesberger et al., 2013;Riccobono et al., 2014;Ehn et al., 2014;Kirkby et al., 2016;Tröstl et al., 2016;Bianchi et al., 2016;Lehtipalo et al., 2018;Rose et al., 2018;Stolzenburg et al., 2018;Mohr et al., 2019;Heinritzi et al., 2020;Yan et al., 2020;Caudillo et al., 2021). These studies found that the functionality and volatility of OOMs are the key factors in determining whether OOM species can participate in NPF (Donahue et al., 2013). More specifically, ultra-low-volatility organic compounds (ULVOCs, whose mass saturation concentrations, C^*, are smaller than $3×10^{-9}$ µg·m^{-3}, or number saturation concentrations, N^*, are smaller than 6 cm^{-3} by assuming an average molar mass of 300 Da) are the main participator of the initial nucleation at certain conditions (Schervish and Donahue, 2020), and extremely-low-volatility organic compounds (ELVOCs, $3×10^{-9} < C^* < 3×10^{-4}$ µg·m^{-3}, $6 < N^* < 6×10^5$ cm^{-3}) and low-volatility organic compounds (LVOCs, $3×10^{-4} < C^* < 0.3$ µg·m^{-3}, $6×10^5 < C^* < 6×10^8$ cm^{-3}) can have a dominant contribution to the growth of newly formed particles.

Owing to the significance of OOMs in atmospheric aerosols formation and growth, its reliable measurement is of high importance. Up till now, the majority of reported sites in the lower troposphere with OOM measurement are non-urban areas, such as forest, agricultural pasture and countryside, where the most abundant OOM species are oxidized products from monoterpenes and isoprene. In the boreal forest of southern Finland, the reported OOM concentration was the highest in summer ($4.6×10^8$ cm^{-3}) (Huang et al., 2020), followed by autumn ($8.0×10^7$ cm^{-3}) (Zha et al., 2018) and spring (~$4.0×10^7$ cm^{-3}) (Yan et al., 2016;Roldin et al., 2019;Bianchi et al., 2017). The level of OOMs also varied significantly at different sites. In Melpitz agricultural-forest of central Europe, OOM concentration ($2.5×10^8$ cm^{-3} in summer) (Mutzel et al., 2015) was comparable with that in Hyytiälä, while in Alabama forest of the United States, OOM concentration was much higher ($4.8×10^9$ cm^{-3} in summer) (Massoli et

al., 2018;Krechmer et al., 2015), possibly due to higher UVB and temperature. Besides, monoterpene OOMs at agricultural-rural mixed Vielbrunn were also detected (3.6×10^6 cm^{-3} in spring), and results showed that many other unidentified species also took a large fraction, especially at night (Kürten et al., 2016). All of these studies highlight the importance of OOM measurement worldwide. Several urban observations were also reported (Brean et al., 2019;Ye et al., 2020). Although they showed that OOMs in Chinese urban cities contain a significant fraction of compounds with 6 to 9 carbons and that many contain nitrogen, they either reported concentrations of a few chosen species or just spectral signals. Moreover, due to the limitation of short measurement periods, they were incapable of exploring the seasonal behavior of OOM concentration and detailed composition, which are crucial for fully evaluating their potential contribution to the growth of SOA.

In this work, we studied the OOMs measured by a CI-APi-ToF mass spectrometer using nitrate (NO_3^-) as reagent ions. The dataset covers four seasons of Year 2019. We performed detailed molecular analyses within the mass to charge ratio between 200-400 Th and identified around 1000 OOMs for each season. The seasonal variations of their concentration, molecular composition, volatility distribution, and potential SOA contribution were systematically investigated for the first time. Furthermore, with a newly developed workflow, we traced their potential sources, including aromatics, aliphatics, monoterpenes, and isoprene. Finally, we evaluated the relative contribution of anthropogenic and biogenic sources in different seasons.

2. MEASUREMENTS AND METHODS

2.1. Measurements

The measurement was conducted at the west campus of Beijing University of Chemical Technology (39.95° N, 116.31° E) on the fifth floor of the teaching building, which is about 15 m above the ground level. This station is a representative urban site, and a detailed description can be found elsewhere (Liu et al., 2020;Yan et al., 2021;Guo et al., 2021).

The concentration of OOMs was measured by a nitrate (NO_3^-)-CI-APi-ToF mass spectrometer (abbreviated as nitrate CIMS) (Aerodyne Research, Inc.). The basic working principle of this instrument can be found elsewhere (Jokinen et al., 2012), and the detailed sampling configuration is the same as that reported by Yan et al. (Yan et al., 2021). Two steps were included in the quantification of OOM concentration. First, a mass-dependent transmission experiment was conducted according to a previous study (Heinritzi et al., 2016), and the transmission curve was obtained by comparing the decrease of primary ion signals and the increase of added perfluorinated acid signals. Second, the calibration factor of sulfuric acid was applied to estimate OOM concentration. Some studies have shown that OOM molecules with less oxygen number are not ionized as efficiently as sulfuric acid by NO_3^- (Hyttinen et al., 2015;Hyttinen et al., 2018;Riva et al., 2019). Therefore, the reported OOM concentration in this study should be regarded as the lower limit. The concentration of each OOM molecule can be calculated as follows:

$$[OOM] = \frac{\sum_{i=0}^{1}(OOM)(HNO_3)_i NO_3^- + (OOM-H)^-(HNO_3)_i}{\sum_{i=0}^{2}(HNO_3)_i NO_3^-} \times C \div T_{OOM}$$

The numerator on the right-hand side is the sum of detected signal of that OOM in the unit of counts per second (cps), either as a cluster of a neutral molecule combined with NO_3^-, $(OOM)(HNO_3)_i NO_3^-$, or as a deprotonated ion, $(OOM-H)^-$. It should be pointed out that in the nitrate CIMS, most OOMs were detected as the cluster form of $(OOM)NO_3^-$, and detailed information can be found in Sect. S1. The denominator is the sum of all reagent ion signals in cps. C is the calibration factor of sulfuric acid, ranging from 6.07×10^9 to 7.47×10^9 cm^{-3} / (normalized cps) during the whole year. Such a narrow range of the calibration factor also indicated that our instrument had a stable performance during the measurement period. T_{OOM} is the relative transmission efficiency of a specific OOM molecule in comparison with that of the reagent ions.

The number concentration of aerosol particles from 6 to 840 nm was measured by a Differential Mobility Particle Sizer (DMPS) (Aalto et al., 2001). The mass concentration of $PM_{2.5}$ was measured with a Tapered Element Oscillating Microbalance Dichotomous Ambient Particulate Monitor (TEOM 1405-DF, Thermo Fisher Scientific Inc, USA). The chemical composition of the $PM_{2.5}$ was obtained from an Aerosol Chemical Speciation Monitor (ACSM) (Jayne et al., 2000;Drewnick et al., 2005), and PMF analysis was further performed to separate secondary organic aerosols from primary ones. Meteorological parameters were measured with a weather station (AWS310, Vaisala Inc.) located on the rooftop of the building. Concentrations of trace gases, including carbon monoxide (CO), sulfur dioxide (SO_2), nitrogen oxides (NO_x), and ozone (O_3), were monitored using Thermo Environmental Instruments (models 48i, 43i-TLE, 42i, 49i, respectively).

The measurement period covers four seasons of the year 2019, including 135 days in total. Winter, spring, summer, and autumn periods range from 5th Jan. to 14th Feb., 15th Mar. to 14th Apr., 10th Jul. to 9th Aug., and 19th Oct. to 18th Nov., respectively.

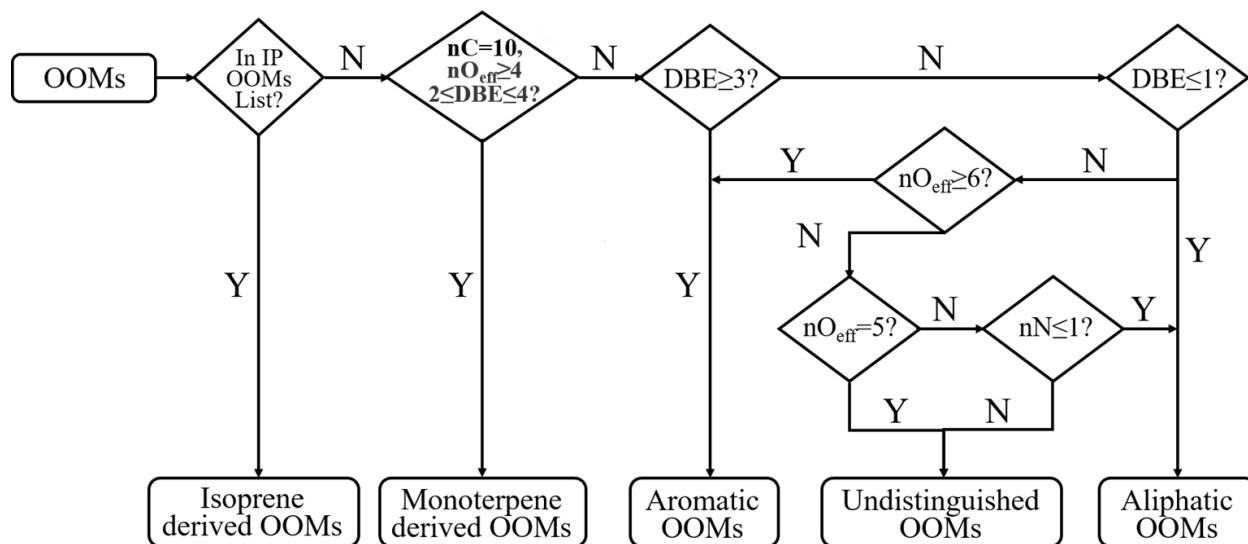## 2.2. A revised workflow for the classification of OOM Sources

A recently developed workflow, based on the molecular composition as well as the up-to-date knowledge of atmospheric OOM formation chemistry, was used for retrieving their possible sources (Xu et al., 2021;Nie et al., 2022). In this approach, mass spectral binning combined with positive matrix factorization (binPMF) (Zhang et al., 2019) needs to be performed first to extract the factor of monoterpene OOMs. However, as performing binPMF is time-consuming and not suitable for large data sets as used in this study, we replaced the binPMF step by the criteria of nC=10, $nO_{eff} \geq 4$, and $2 \leq DBE \leq 4$ (Fig. 1) for the selection of monoterpene OOMs. Such standards were set based on their reported composition (Ehn et al., 2012;Yan et al., 2016;Jokinen et al., 2014;Boyd et al., 2015;Berndt et al., 2016;Berndt et al., 2018). Here, nC is the carbon number. nO_{eff} (= $nO - 2 \times nN$) is the effective oxygen number, which subtracts the number of oxygen bonded to nitrogen by assuming that all nitrogen atoms are in the form of nitrate groups ($-ONO_2$) or peroxynitrate nitrate group ($-OONO_2$). To our best knowledge, this is the common case

150 for all nitrogen-containing compounds formed through the reaction between RO_2 and NO_x (Orlando and Tyndall,

151 2012;Seinfeld and Pandis, 2016). Exceptions are those nitrophenols (Yan et al., 2016;Wang et al., 2019;Song et al.,

152 2021) that were classified separately (Nie et al., 2022) . The reason for choosing nO_{eff} rather than nO is that it better

153 reflects the oxidation state of closed-shell molecules as well as their parent RO_2 radicals. For example, $C_7H_9O_5$

154 peroxy radical can produce both $C_7H_{10}O_4$ and $C_7H_9O_6N$ when reacting with NO, and all of them have the same nO_{eff}

155 of four. In addition, nO_{eff} considers the influence of nitrogen and represents volatility more directly (Yan et al.,

156 2020), and thus makes it easier for the volatility comparison among OOMs with different nitrogen atoms.

157 DBE denotes the double bond equivalence and is calculated as (2nC+2–nH–nN)/2, which is the same as the term

158 degree of unsaturation. The DBE of one OOM molecule is influenced by both its precursor and the oxidation

159 processes. For example, aromatic VOCs have DBE values no smaller than 4. For their oxidation products, a previous

160 study has shown that under OH exposures equivalent to approximately 10 h to 15 days in typical atmospheric

161 conditions, they possess DBE values no smaller than 2 (Garmash et al., 2020). However, reported monoterpene

162 OOMs also have DBE values the same as aromatic OOMs, which makes them difficult to distinguish. According

163 to laboratory studies, the majority of monomer products from monoterpene oxidation are C10 compounds (Yan et

164 al., 2020). Measurement results also showed that the concentrations of C10 aromatic VOCs are very low (Zhang et

165 al., 2017) compared with other C6-C9 ones. Therefore, those C10 OOMs with DBE values of 2 to 4 are likely

166 monoterpene OOMs. For OOMs with DBE values smaller than 2, neither aromatics nor monoterpenes oxidation

167 could explain their formation. Hence, the precursors of those OOMs should be the ones without aromatic rings and

168 have smaller DBE values, such as alkanes, alkenes, and some unsaturated oxygen-containing VOCs (OVOCs).

169 OOMs with DBE values of 2 are rather complex. Their precursors could be aromatics, aliphatics, or other unknown

170 sources, and a detailed discussion of the classification criteria can be found in Nie et al. (Nie et al., 2022).

171 Due to the complexity of atmosphere, there indeed remain some uncertainties in the workflow. For example, a

172 recent study found that some aliphatic VOCs were able to produce OOMs with DBE values of 2 – 3 and nO_{eff} no

173 smaller than 6 (Wang et al., 2021), which however, are classified as aromatic OOMs in the workflow. Nie et al.

174 (Nie et al., 2022) has tested the performance of the workflow on OOMs from Wang et al. 2021. Results show that

175 the accuracy is almost 100 % for OOMs from *n*-decane and ~ 75 % for OOMs from cyclohexane (Nie et al., 2022).

176 Thus, the workflow is generally reliable in classifying aliphatic OOMs. In addition, the VOC to NO_x ratios in the

177 experiments of Wang et al. (Table S17) is much higher than in urban Beijing (Table S18). This high-level NO_x

178 might suppress the autoxidation as the RO_2 + NO termination reaction likely dominates the fate of RO_2 radicals,

179 leading to comparatively lower nO_{eff}. In this way, aliphatic OOMs is difficult to reach nO_{eff} of 6. The revised

180 workflow finally divided OOMs into five groups: isoprene (IP) OOMs, monoterpene (MT) OOMs, aromatic OOMs,

181 aliphatic OOMs, and a small amount of undistinguished OOMs (6-9 %) that cannot be classified into those four

182 types.

OOMs → In IP OOMs List? —N→ nC=10, nO$_{eff}$≥4 2≤DBE≤4? —N→ DBE≥3? —N→ DBE≤1?

nO$_{eff}$≥6? (Y← , N←)

nO$_{eff}$=5? —N→ nN≤1? —Y→

Y / N

Isoprene derived OOMs | Monoterpene derived OOMs | Aromatic OOMs | Undistinguished OOMs | Aliphatic OOMs

Figure 1. Workflow for retrieving OOM sources. "IP OOMs" represents isoprene-derived OOMs. nO$_{eff}$ and nN are the numbers of effective oxygen and nitrogen in each OOM molecule, respectively. "Y" and "N" denote "Yes" and "No", respectively.

3. RESULTS AND DISCUSSIONS

3.1. Seasonal Variation of OOM Concentration and Composition

The concentration and molecular composition are the most fundamental characteristics of OOMs. We summarized the OOM concentrations in Beijing and other lower tropospheric sites in Table 1 and Fig. 2 for better comparison. Generally, a clear seasonal trend of OOM concentration in Beijing can be observed, where total OOM concentration is highest in summer ($1.6×10^8$ cm^{-3}), followed by autumn ($7.9×10^7$ cm^{-3}) and spring ($5.7×10^7$ cm^{-3}), and the lowest in winter ($2.3×10^7$ cm^{-3}). This apparent increase of OOM concentrations with an increased temperature and theoretical global radiation indicates that elevated solar radiation along with higher temperature favors the generation of OOMs. In comparison to other locations, the level of OOMs in urban Beijing varied within the ranges of previously reported ones (Yan et al., 2016;Roldin et al., 2019;Bianchi et al., 2017;Zha et al., 2018;Huang et al., 2020;Mutzel et al., 2015;Massoli et al., 2018;Nie et al., 2022). Interestingly, the above clear correlation between global radiation (or temperature) and OOM concentration can also be seen in other locations, yet OOMs in forest environments are in general higher than in urban or suburban areas. On the one hand, this observation suggests that OOM formation at a specific environment is prevailingly influenced by the strength of atmospheric photochemistry; on the other hand, forest environment appears to have more abundant OOMs than urban environments, possibly because the OOM yield of biogenic VOCs is higher than that of anthropogenic VOCs (Berndt et al., 2016;Teng et al., 2017;Garmash et al., 2020;Molteni et al., 2018). Yet, a quantitative explanation of the OOM variation between seasons and locations requires comprehensive measurements as well as analyses on both the production and loss of OOMs.

Table 1. Mean, standard deviation (Std), median, 25 and 75 percentiles (25th and 75th) of measured OOM concentrations at various lower tropospheric sites.

Measurement Site	Period	Mean (cm^{-3})	Std (cm^{-3})	Median (cm^{-3})	25th (cm^{-3})	75th (cm^{-3})	Reference
Beijing, China	2019 Jan.-Feb.	2.7×10^7	1.7×10^7	2.3×10^7	1.3×10^7	3.6×10^7	This study
Beijing, China	2019 Mar.-Apr.	6.9×10^7	5.1×10^7	5.7×10^7	3.1×10^7	8.9×10^7	This study
Beijing, China	2019 Jul.-Aug.	1.6×10^8	7.5×10^7	1.6×10^8	1.1×10^8	2.2×10^8	This study
Beijing, China	2019 Oct.-Nov.	8.3×10^7	5.2×10^7	7.9×10^7	4.0×10^7	1.2×10^8	This study
Hong Kong, China	2018 Nov.	2.3×10^8	1.1×10^8	2.1×10^8	1.5×10^8	2.9×10^8	2022, Nie et al.
Shanghai, China	2018 Nov.	7.8×10^7	6.3×10^7	6.1×10^7	2.6×10^7	1.2×10^8	2022, Nie et al.
Nanjing, China	2018 Nov.	7.7×10^7	5.4×10^7	7.2×10^7	3.1×10^7	1.1×10^8	2022, Nie et al.
Hyytiälä forest, Finland	2012 Apr.-May	7.5×10^7	6.1×10^7	5.7×10^7	3.6×10^7	9.2×10^7	2016, Yan et al.
Hyytiälä forest, Finland	2013 May	1.4×10^7	7.9×10^6	1.2×10^7	8.1×10^6	1.8×10^7	2019, Roldin et al.
Hyytiälä forest, Finland	2013 Apr.-Jun.	4.5×10^7	1.2×10^7	4.9×10^7	3.2×10^7	5.5×10^7	2017, Bianchi et al.
Hyytiälä forest, Finland	2016 Sep.	1.2×10^8	1.0×10^8	8.0×10^7	3.8×10^7	1.7×10^8	2018, Zha et al.
Melpitz, Germany	2013 Jul.	2.7×10^8	1.7×10^8	2.5×10^8	1.4×10^8	3.5×10^8	2015, Mutzel et al.
Alabama forest, USA	2013 Jun.-Jul.	4.7×10^9	1.5×10^9	4.8×10^9	3.7×10^9	5.3×10^9	2018, Massoli et al.
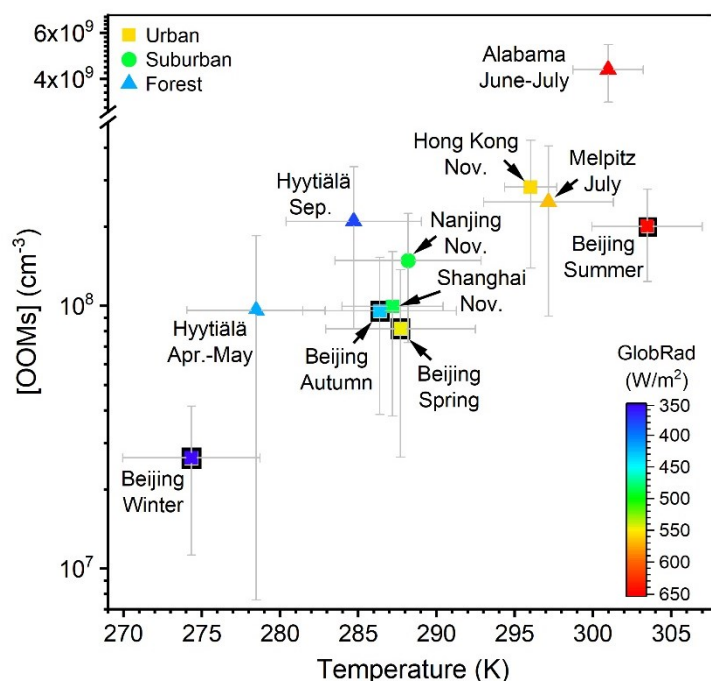
Figure 2. OOM concentration vs. temperature at various lower tropospheric sites during daytime (07:00 – 17:00). Data points are colored by theoretical global radiation (GlobRad). Square, circle, and triangle markers represent urban, suburban, and forest areas, respectively. The gray error bars show standard deviations (1σ). Nanjing, Shanghai and Hong Kong datasets are from Nie et al. (Nie et al., 2022) , Melpitz data is from Mutzel (Mutzel et al., 2015), Alabama data is from Massoli et al. (Massoli et al., 2018), and Hyytiälä datasets are from Yan et al. (Yan et al., 2016) and Zha et al (Zha et al., 2018).

To further demonstrate the seasonal influence of solar radiation and precursor VOCs on OOM concentration, we classified OOMs of each season into four groups based on the brightness parameter (Dada et al., 2017) and PM$_{2.5}$ level, respectively. As shown in Fig. S6, in seasons other than summer, OOM concentration under polluted conditions is much higher than that under clean conditions, which likely results from the elevation of precursors coming along with polluted air masses and the accumulation during the pollution. Besides, the concentration of

219 total OOMs on sunny days is higher than that on cloudy days, implying that photochemical oxidation plays a key

220 role in the production of OOM molecules. There is one exception that OOM concentration is not significantly

221 different between sunny and cloudy days under clean condition in autumn, and the cause cannot be concluded in

222 this study without a complete VOC measurement.

223   For OOM composition, the two-dimensional H/C-O_{eff}/C (ratio of hydrogen number to carbon number vs. ratio

224 of effective oxygen number to carbon number) diagrams are plotted to show its characteristics (Fig. S7). And main

225 CHO, CHON, and $CHON_2$ OOM species are also summarized in Table 2. Generally, the composition of OOM

226 molecules exhibits high similarity among different seasons, suggesting no significant changes in OOM formation

227 in general. However, two seasonal characteristics can be found. First, the most oxygenated OOM molecules, such

228 as $C_nH_{2n-2}O_{6,7}$, $C_nH_{2n-4}O_{7,8}$, $C_nH_{2n+1}O_8N$ and $C_nH_{2n-1}O_9N$ OOMs, are mainly observed in summer, and meanwhile,

229 the least oxygenated ones, e.g., $C_nH_{2n-7}O_2N$ and $C_nH_{2n-9}O_{4,5}N$ are mostly detected in winter. These observations

230 indicate that, in addition to the enhanced OOM concentration, strong photochemistry also leads to a high oxidation

231 state of OOM. And these summer-specific OOMs can be classified as highly oxygenated organic molecules (HOMs).

232 Second, $C_5H_{10}O_8N_2$ is exceedingly high in summer. A previous study suggested that $C_5H_{10}O_8N_2$ is one dominant

233 oxidation product from isoprene (Xu et al., 2021), and therefore, the high concentration of $C_5H_{10}O_8N_2$ is a clear

234 indication of intensive isoprene oxidation in summer, which will be discussed in detail in Sect. 3.2.

235 **Table 2.** Main CHO, CHON and $CHON_2$ OOM species measured in this study.

DBE	CHO OOMs	CHON OOMs	$CHON_2$ OOMs
0	$C_nH_{2n+2}O_6$	$C_nH_{2n+1}O_{3-8}N$	$C_nH_{2n}O_{4-11}N_2$
1	$C_nH_{2n}O_{2-8}$	$C_nH_{2n-1}O_{3-9}N$	$C_nH_{2n-2}O_{4-10}N_2$
2	$C_nH_{2n-2}O_{3-7}$	$C_nH_{2n-3}O_{3-9}N$	$C_nH_{2n-4}O_{5-11}N_2$
3	$C_nH_{2n-4}O_{2-8}$	$C_nH_{2n-5}O_{3-10}N$	$C_nH_{2n-6}O_{8-11}N_2$
4	$C_nH_{2n-6}O_{3-9}$	$C_nH_{2n-7}O_{3-9}N$	$C_nH_{2n-8}O_{7,8}N_2$
5	$C_nH_{2n-8}O_{3-8}$	$C_nH_{2n-9}O_{4-10}N$	$C_nH_{2n-10}O_{6-10}N_2$

236   For a better understanding of OOM composition variation among seasons, the distributions of nC, nO_{eff}, nN, and

237 DBE, as well as their seasonal variations, are further analyzed. It should be pointed out that the concentration

238 (5.3×10^7 cm^{-3}) and the fraction (33 %) of IP OOMs in summer is much higher than those in other three seasons, and

239 therefore they are plotted in bars with diagonal lines individually (Fig. 3). In terms of carbon content, the majority

240 of OOMs contain 5 to 10 carbon atoms. For OOMs with 6 to 10 carbon atoms, in seasons other than summer, C6

241 are the most abundant, and a decreasing trend can be seen along with an increasing nC, while in summer, an opposite

242 trend is observed, i.e., the relative contribution increases with an increasing nC. The causes behind the different

243 trends in summer and other seasons are complex but might include changes in the precursor VOC distribution,

244 varying reactivity responses of VOCs to temperature, and the volatilities of OOMs that influence their atmospheric

245 lifetime. Further analysis on this topic will be made in the future. For C5 OOMs, the contribution from isoprene

246 varies from less than half in winter and spring to ~70 % in summer. The high contribution of IP OOMs in summer

247 is in line with the strong isoprene emission coupled with the enhanced photo-oxidation (Cheng et al., 2018;Zhang

248 et al., 2020).

249 Concerning the oxygen content, most OOMs contain 3 to 7 effective oxygen atoms, accounting for 86-95 % of

250 total OOMs in all seasons. With the increase of effective oxygen number, the contribution of corresponding OOMs

251 first increases and then decreases, with nO_{eff}=4 OOMs having the highest fraction. Fig. S8 shows that the

252 concentration-weighted average nO_{eff} is the highest in summer and lowest in winter and autumn, which is consistent

253 with the observation of individual molecules where the most highly oxygenated ones are usually more abundant in

254 summer. The enhanced multi-step oxidation (Garmash et al., 2020;Wu et al., 2021) and favored auto-oxidation

255 (Molteni et al., 2018;Wang et al., 2017;Wang et al., 2018b;Bianchi et al., 2019) at high temperatures in warmer

256 seasons are most likely the causes. Furthermore, when taking IP OOMs into account, nO_{eff}=4 becomes even more

257 prominent in summer, in which $C_5H_{10}O_8N_2$ takes the largest portion and accounts for 77 % of nO_{eff}=4 IP OOMs. In

258 winter and autumn, however, nO_{eff}=3 has a much higher fraction than those in the other two seasons, and those

259 OOMs are mainly composed of low-DBE compounds, such as $C_nH_{2n}O_7N_2$, $C_nH_{2n-2}O_7N_2$, and $C_nH_{2n-1}O_5N$ species.

260 As for nitrogen content, the vast majority (98-99 %) of OOMs contain 0 to 2 nitrogen atoms, in which CHON

261 OOMs take the largest fraction, varying from 42 % to 51 % among seasons. It should be noted that, although the

262 mixing ratios of NO_x in different seasons change significantly, the nitrogen distributions of non-isoprene OOMs are

263 similar, which is probably due to the fact that NO (0.6-10.0 ppbv) and NO_2 (8.9-28.3 ppbv) concentrations in urban

264 Beijing are always high throughout the year. Those nitrogen atoms could come from either NO_3 radical oxidation

265 or NO_x termination. During the day, nitrogen is likely added mainly through NO_x termination as NO_3 radical should

266 be photolyzed or titrated by NO. However, in the absence of NO_3 photolysis at night, when NO concentration is

267 low, the concentration of NO_3 radical could reach up to ~10 pptv (2.7×10^8 cm^{-3}) in Beijing (Wang et al., 2018a).

268 Under such levels, the NO_3 radial could even dominate the oxidation of biogenic VOCs (i.e., isoprene and

269 monoterpenes) and some aliphatic VOCs, yet the oxidation of aromatic VOCs are driven by OH radicals (Table S4

270 and Table S5). Therefore, nitrogen is possibly added through both processes at night.

271 In the case of DBE distribution, most OOMs comprise 0 to 6 DBE values and there is not too much difference

272 among seasons for non-isoprene OOMs. Generally, with the increase of DBE, the fraction of corresponding non-

273 isoprene OOMs first increases and then decreases, with DBE=2 OOMs having the highest contribution (20-29 %).

274 And this is possibly caused by the fact that almost all precursor VOCs, such as aromatics, aliphatics and

275 monoterpenes, can form oxidation products with DBE value of 2. OOMs with DBE larger than 4 and nC no smaller

276 than 10 are likely derived from polycyclic aromatic hydrocarbons (PAHs, DBE≥7), and their fraction varies from

277 5 % in summer to 7-8% in the other three seasons. This demonstrates that PAHs may also have a non-negligible

278 contribution to total OOMs. For IP OOMs, most of them possess 0 or 1 DBE, and only a small fraction (2-16 %) of

279 them retains DBE of precursor isoprene. This indicates that hydroxyl or hydroperoxyl are the major functional

280 groups of these products, whereas products with higher DBE values are not prominent. It could mean that

281 compounds containing carbonyl or epoxide groups are either not efficiently formed under the urban environment,

282 or fast lost via heterogeneous reactions (Riedel et al., 2015;Zhang et al., 2022). Meanwhile, the instrumental

283 detection bias, i.e., nitrate CIMS is less sensitive to carbonyl and epoxide groups, cannot be excluded. Therefore,

284 further combination of CIMS instruments with different chemical ionization methods are highly desirable in the

285 future.
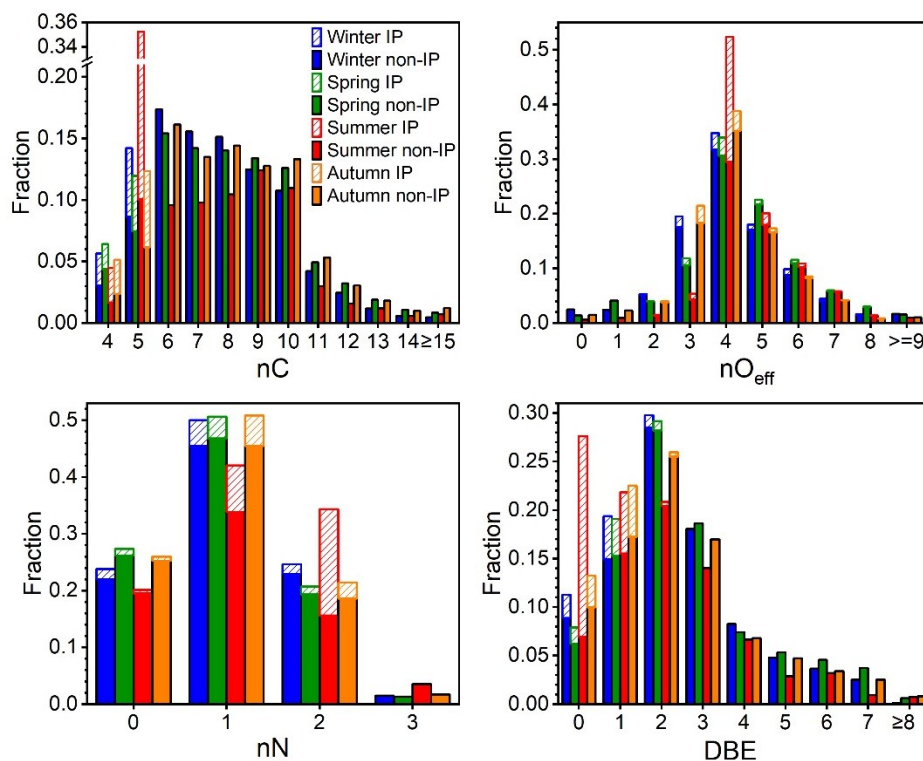
286
287 **Figure 3.** Number of carbon (nC), effective oxygen (nO_{eff}), nitrogen (nN), and double bond equivalence (DBE) distribution of
288 OOMs for four seasons. The abbreviations "IP" and "non-IP" represent IP OOMs and other non-isoprene OOMs, respectively.
289 The bars with diagonal lines and filled colors represent IP OOMs and non-isoprene OOMs, respectively.

290 **3.2. Characteristics of Source-classified OOMs**

291 With the workflow described in Sect.2.2, total OOMs were classified into four types: IP OOMs, MT OOMs,

292 aromatic OOMs, and aliphatic OOMs. As shown in Fig. 4, the seasonal concentrations of OOMs from different

293 sources vary with the same trend, highest in summer, followed by autumn, spring, and winter. During the whole

294 year, aromatic OOMs (29-41 %) and aliphatic OOMs (26-41 %) are the most abundant categories, demonstrating

295 that OOMs in Beijing are dominantly from anthropogenic sources. This is also consistent with the observation of

296 SOA composition in previous studies (Le Breton et al., 2018;Mehra et al., 2021). In terms of OOMs from biogenic

297 sources, IP OOMs show a prominent contribution in summer (33 %), which is much higher than those in other

298 seasons (8-10 %). Although it is recently suggested that isoprene can have both biogenic and anthropogenic sources

299 (Wagner and Kuttler, 2014;Panopoulou et al., 2020), the much higher enhancement of IP OOMs in summer can

300 only be explained by the large additional biogenic emission (Cheng et al., 2018;Mo et al., 2018). For MT OOMs,

however, the fractional contribution does not show a seasonal variation as clear as that of IP OOMs – it only varies between 5 % and 6 %.
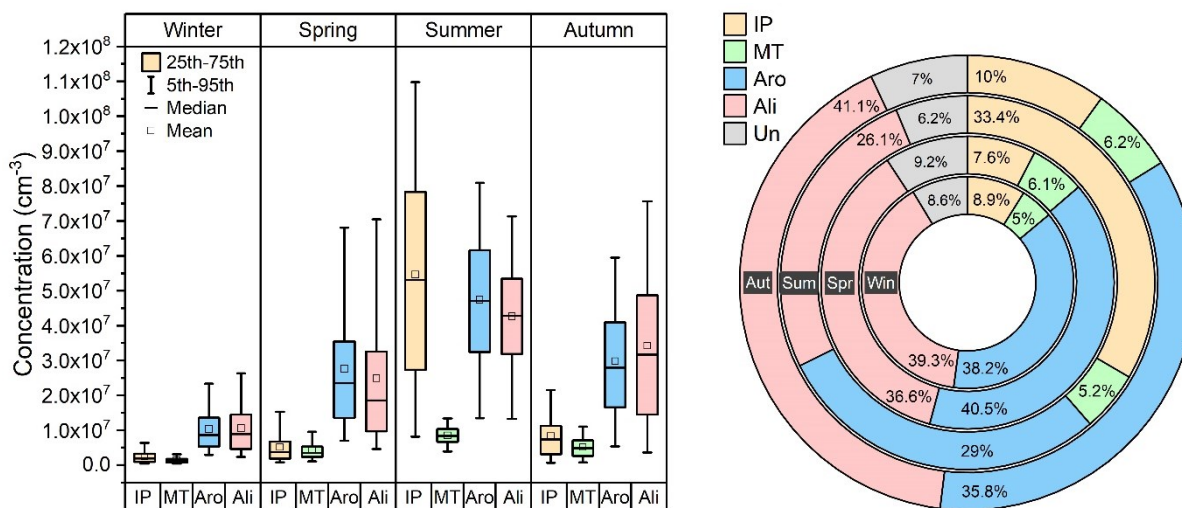
Figure 4. Concentration (left panel) and fraction (right panel) of source-classified OOMs in four seasons. The abbreviations "IP" "MT" "Aro" "Ali" and "Un" stand for IP OOMs, MT OOMs, aromatic OOMs, aliphatic OOMs and undistinguished OOMs respectively. "Win" "Spr" "Sum" and "Aut" represent winter, spring, summer and autumn separately.

3.2.1 Characteristics of biogenic OOMs

The spectral profiles and the fractions of IP OOMs with different nitrogen numbers in four seasons are shown in Fig. 5. Prominent IP OOM species include $C_4H_6O_4$, $C_5H_8O_4$, $C_4H_7O_{6,7}N$, $C_5H_9O_{5-7}N$, $C_5H_{10}O_{7,8}N_2$ and $C_5H_9O_{10}N_3$. $CHON_3$ OOM ($C_5H_9O_{10}N_3$) is detected in all four seasons, suggesting that multi-generation oxidation is involved throughout the year. Besides, the composition of IP OOMs exhibits clear seasonal variation. First, compared with other three seasons, $C_5H_{10}O_8N_2$ and $C_5H_9O_{10}N_3$ have much higher contributions in summer, indicating that NO_x may be involved more efficiently in the oxidation process of isoprene despite its lower concentration (Fig. S10 and Table S1). In addition, nighttime NO_3 radicals produced efficiently during summer nights (Wang et al., 2018a) should also promote their formation. Second, despite the overall lowest concentrations of IP OOMs in winter, $C_4H_8O_7$ exhibits a maximum concentration (Fig. S9) and the highest fraction, implying that it may has additional sources other than isoprene oxidation in winter. Third, due to the influence of $C_5H_{10}O_8N_2$ and $C_5H_9O_{10}N_3$, $CHON_2$ and $CHON_3$ IP OOMs take extremely large proportion (~ 67 %) in summer. And interestingly, the seasonal trend of nitrate IP OOM fraction (from largest to smallest is summer, autumn, spring and winter) did not follow the variation of NO_x concentration (from highest to lowest is autumn, winter, spring and summer, Fig. S5 and Table S1), which suggests that the formation of nitrate IP OOMs probably has a non-linear response to NO_x.

The concentrations of these prominent IP OOM molecules during summertime in Beijing, Nanjing (32.12° N, 118.95° E) (Liu et al., 2021) and Alabama mixed-forest (32.90° N, 87.25° W) (Krechmer et al., 2015;Massoli et al., 2018) are further compared (Fig. 6). Please note that these molecules plotted are not all the IP OOMs but rather selected abundant ones reported in the literature and in this study. As shown in Fig. 6 (A), IP OOMs exhibit the

highest concentration in Alabama forest and the lowest one in Beijing, and the level of IP OOMs in Beijing and Nanjing are comparable. This concentration difference is likely caused by the variation of biogenic isoprene emissions, since Alabama measurement was conducted in a forest, Nanjing site is a suburban area with large vegetation coverage nearby, and Beijing site is located in urban downtown. Besides, the overall varying patterns of IP OOM species in Beijing and Nanjing are very similar, indicating that isoprene in those two urban sites undergo similar oxidation pathways. In terms of oxygen distribution, Beijing and Nanjing are rather similar in that $nO_{eff}=4$ OOMs contribute the most, whereas in Alabama $nO_{eff}=5$ ones are the most abundant (Fig. 6 (B)). This lower oxygen content in urban cities is probably caused by the high NO_x levels (11.1 ppbv, 8.5 ppbv and 0.5 ppbv for Beijing, Nanjing and Alabama respectively, Fig. S10), since NO_x efficiently suppresses the oxygen addition of RO_2 radicals (Zhao et al., 2018). Furthermore, the different NO_x levels among the three sites also influence the nitrogen content that Beijing is the highest and Alabama is the lowest (Fig. 6 (C)).

From the perspective of diurnal variation, CHO IP OOMs in Beijing possess one daytime peak, while CHON OOMs mainly contain day-night-dual-peak or nocturnal-peak-only types (Fig. S11), which is similar to that reported in Alabama forest (Massoli et al., 2018). But it should be noted that the diurnal variations of some CHON IP OOMs with same molecular composition in this study and Massoli et al. (2018) are not identical, suggesting that their formation pathways are different under various atmospheric conditions.
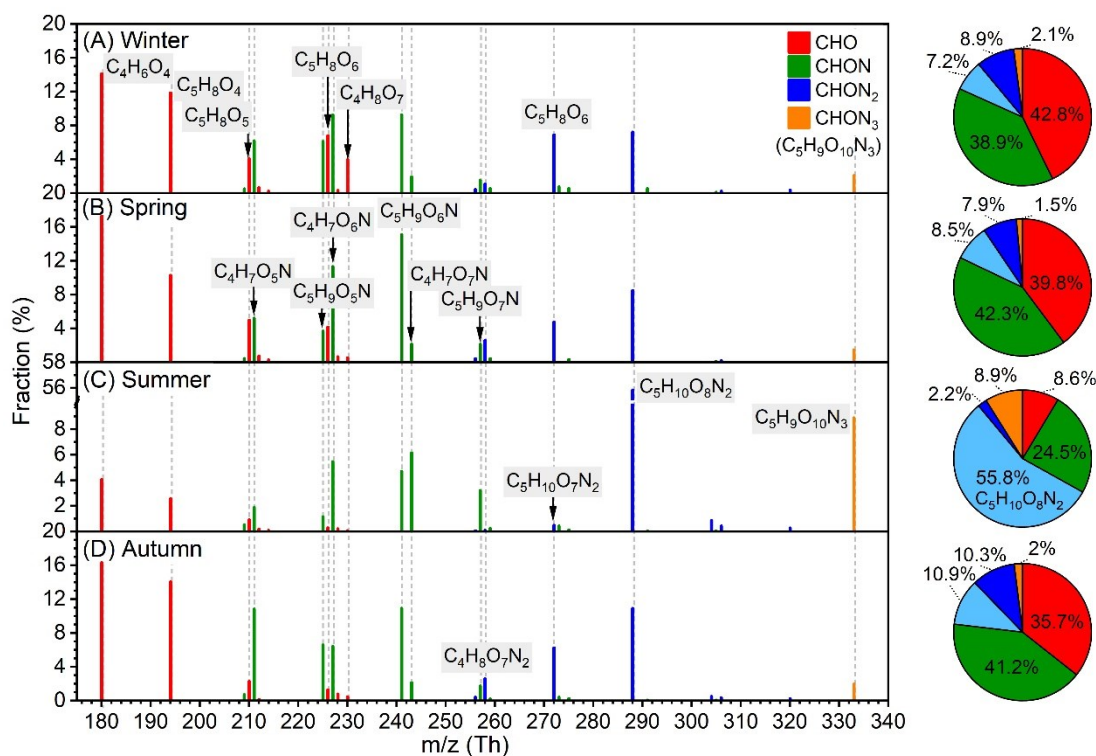
Figure 5. Fractional profiles of each IP OOM molecule in (A) winter, (B) spring, (C) summer and (D) autumn. The mass to charge ratio (m/z) denotes OOM clustered with NO_3^- or as deprotonated ones. The fraction of each compound is calculated as the ratio of its concentration to the total concentration of IP OOMs. The red, green, blue and orange bars are for CHO, CHON, $CHON_2$ and $CHON_3$ OOMs respectively. Please note that $CHON_3$ OOMs only include $C_5H_9O_{10}N_3$.
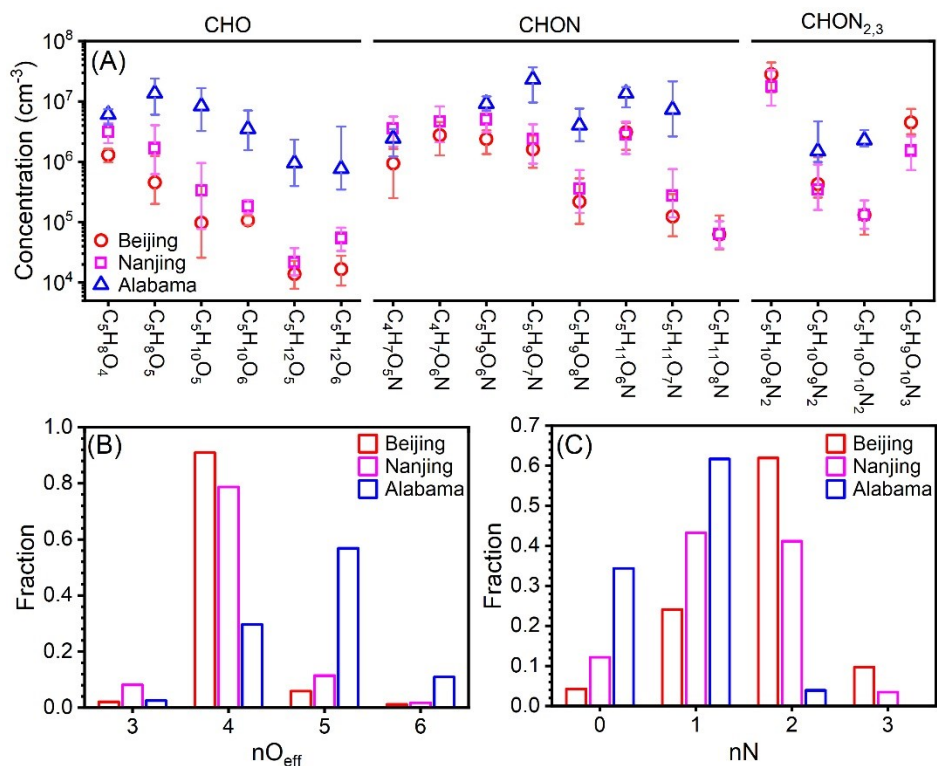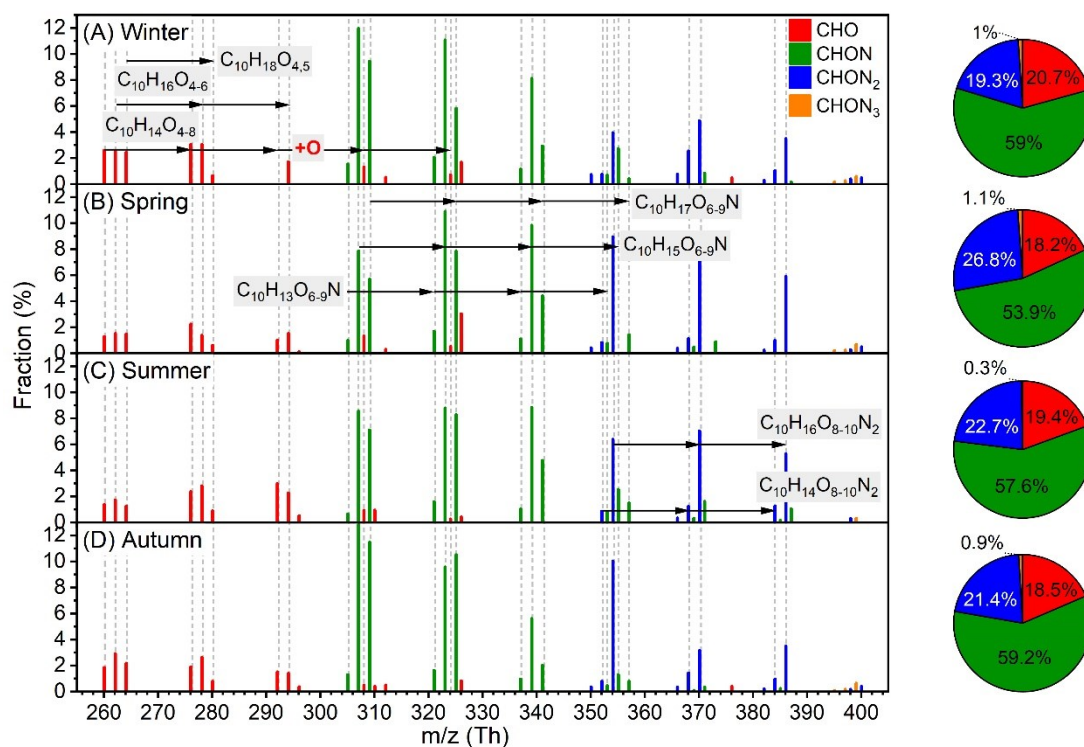
Figure 6. (A) Concentration comparison of specific fingerprint IP OOM molecules between our study and previously reported ones (Krechmer et al., 2015;Massoli et al., 2018;Liu et al., 2021). The markers are median concentration values, and the bottom and up ranges of the error bars denote 25th and 75th percentiles respectively. Distribution of (B) effective oxygen number, nO_{eff}, and (C) nitrogen number, nN, of IP OOMs plotted in figure (A).

Different from IP OOMs, the overall composition distributions of MT OOMs in the four seasons are quite similar and vary with identical oxygen addition patterns (Fig. 7). Predominant MT OOM molecules are $C_{10}H_{14}O_{4-8}$, $C_{10}H_{16}O_{4-6}$, $C_{10}H_{18}O_{4,5}$, $C_{10}H_{13,15,17}O_{6-9}N$ and $C_{10}H_{14,16}O_{8-10}N_2$. Besides, most MT OOMs belong to CHON category (54-59 %), and the CHO (18-21 %) and $CHON_2$ (19-27 %) ones, with a comparable contribution during the year.

Then, for a better understanding of MT OOM characteristics under different atmospheric environments, representative MT OOM molecules in summer Beijing, spring Hyytiälä forest (61.8° N) (Yan et al., 2016) and summer Alabama mixed-forest (Massoli et al., 2018) are further compared. The following differences can be identified. First, MT OOM concentrations are the highest in Alabama and the lowest in urban Beijing (Fig. 8 (A)), which should result from the synergetic influence of UVB, temperature and precursor monoterpenes. Second, the levels of the two MT radicals that have high concentrations in the Hyytiälä forest, $C_{10}H_{15}O_8\cdot$ and $C_{10}H_{15}O_{10}\cdot$, are not detected in Beijing. This is possibly caused by both low monoterpene abundance (Cheng et al., 2018) and high NO_x concentration in Beijing (11.06 ppbv, Fig. S10), which lead to a low production rate and high loss rate of RO_2 radicals. Third, most MT OOMs in urban Beijing possess 5 or 6 effective oxygen, whereas in the forest environment a large fraction of them can hold 7 to 10 effective oxygen (Fig. 8 (B)). This again suggests that high NO_x in Beijing effectively inhibits the oxygen addition processes (Zhao et al., 2018;Orlando and Tyndall, 2012). Additionally, high NO_x in Beijing also leads to high nitrogen content (Fig. 8 (C)) by promoting the termination reaction between RO_2

368 and NO_x (Orlando and Tyndall, 2012) and facilitating the formation of NO_3 radical (Wang et al., 2018a), which

369 further leads to the formation of nitrate MT OOMs (Boyd et al., 2015;Nah et al., 2015).

370
371 **Figure 7.** Fractional profiles of each MT OOM molecule in (A) winter, (B) spring, (C) summer and (D) autumn. The mass to
372 charge ratio (m/z) denotes OOM clustered with NO_3^- or as deprotonated ones. The fraction of each compound is calculated as
373 the ratio of its concentration to the total concentration of MT OOMs. The red, green, blue and orange bars are for CHO, CHON,
374 $CHON_2$ and $CHON_3$ OOMs respectively.
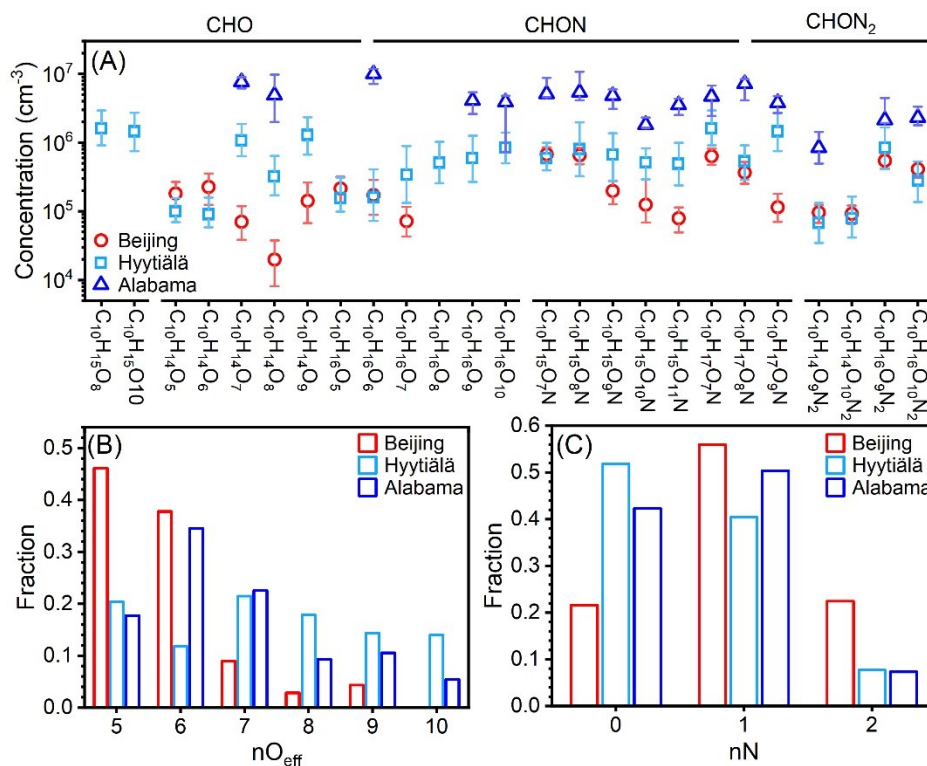
Figure 8. (A) Concentration comparison of specific fingerprint MT OOM molecules between our study and previously reported ones (Massoli et al., 2018;Yan et al., 2016). The markers are median concentration values, and the bottom and up ranges of the error bars denote 25th and 75th percentiles respectively. Please note that only the summer Beijing data was plotted as the overall pattern of MT OOMs in Beijing summer and spring are very similar (Fig. 7). Distribution of (B) effective oxygen number, nO_{eff}, and (C) nitrogen number, nN, of MT OOMs plotted in figure (A).

3.2.2 Characteristics of anthropogenic OOMs

Although the oxidation pathways and product composition of a few aromatic VOCs have been studied previously, the reported products are of much less diversity compared to the complex real atmosphere. Therefore, we rely on the workflow (see Sect. 2.2 and (Nie et al., 2022)) to find out possible aromatic OOMs in our measurement. Among the deduced aromatic OOMs, almost all C6-C9 CHO and C6 CHON compounds have been detected in previous benzene, toluene, xylene, ethylbenzene and mesitylene experiments (Molteni et al., 2018;Garmash et al., 2020) (see detail in Table S9), which demonstrates the reliability of our workflow.

As shown in Fig. 9 (A) to (D), predominant aromatic species in different seasons possess high similarity and they could be classified into $C_{6-9}H_{8-14}O_4$, $C_{6-8}H_{8-12}O_5$, $C_{7,8}H_{8,10}O_5$, $C_{6-10}H_{7-15}O_6N$, $C_{7-9}H_{9-13}O_7N$, $C_{8-10}H_{11-15}O_8N$ and $C_{8,9}H_{12-14}O_{10}N_2$ categories, among which a prominent CH_2 spacing is seen. Such patterns are most likely due to the co-existence of homologous precursor VOCs, although fragmentation processes during the oxidation could also play a role (Pan and Wang, 2014;Zaytsev et al., 2019;Xu et al., 2020). Besides, the distribution of CHON aromatic OOMs in winter and autumn are very similar, with $C_8H_{11}O_6N$ being the highest; in comparison, the overall distribution moves to higher oxygen content in summer, e.g., $C_8H_{11}O_7N$ becomes the largest one. This suggests that enhancement of radiation, which leads to strong photochemistry and high temperature, and the reduction of NO_x in

summer benefit the formation of highly oxygenated organic molecules (Garmash et al., 2020;Orlando and Tyndall, 2012). There are also fingerprint molecules for different seasons, such as $C_{10}H_8O_6$ in spring, $C_9H_{10}O_{11}N_2$ in summer, and $C_{10}H_6O_4$ in summer and autumn. Due to the complexity of real atmosphere, the reason for their seasonal variation is unclear, and further analysis is warranted. In terms of nitrogen content, aromatic OOMs contain large fraction of CHO (42-52 %) and CHON (39-51 %) species. The contribution of $CHON_2$ OOMs reaches the highest in summer, which again indicates that the involvement of NO_x is enhanced under the influence of elevated UVB and temperature. The carbon distribution among seasons are very similar (Fig. S13), where C4 to C9 aromatic OOMs, probably derived from monocyclic aromatic hydrocarbons, make up 68-76 %, and other C≥10 ones, of which 59-68 % are likely the oxidation products from PAHs (DBE≥5) (Table S10), take up 24-32 %. This implies that the relative abundance of emitted aromatic precursors with different carbon atoms is quite stable during the year.

Major aliphatic OOM molecules in different seasons are highly similar, and they possess more evident homologous patterns than aromatic OOMs (Fig. 9 (E) to (H) and Table S11). The dominant species of aliphatic OOMs are $C_{6-9}H_{10-16}O_4$, $C_{6-10}H_{11-19}O_6N$, $C_{5-10}H_{7-17}O_6N$, $C_{5-10}H_{8-18}O_8N_2$ and $C_{6-9}H_{12-18}O_7N_2$, and some less oxygenated compounds, e.g., $C_{6-8}H_{11-15}O_5N$, also have considerable contributions in winter and autumn. For nitrogen content, CHO aliphatic OOMs only take a small fraction of 8-11 %, implying that NO_x termination may dominate the formation of aliphatic close-shell molecules. Meanwhile, this CHO OOM fraction of aliphatic OOMs is much smaller than that of aromatic OOMs (42-52 %), suggesting that the branching ratio of aliphatic RO_2 - NO_x reaction forming $CHON_x$ species is higher than that of the aromatic one. Besides, unlike aromatic OOMs, aliphatic $CHON_2$ OOMs have a bigger contribution in winter than in the other three seasons. This is because a major sequence of $CHON_2$ OOMs, $C_{6-14}H_{12-28}O_7N_2$, is found to be coincided with $PM_{2.5}$ (Fig. S14), which is frequently high in winter. In winter Beijing, the regional transportation of air masses from the south and southeast areas is a large source of $PM_{2.5}$ (Wang et al., 2015;Chen et al., 2021;Chen et al., 2022;Tan et al., 2022), therefore, the good correlation between $CHON_2$ species and $PM_{2.5}$ suggests that those compounds might also have regional sources. Table S12 shows that $C_{6-10}H_{12-20}O_7N_2$ are relatively volatile and are classified as semi-volatile organic compounds, thus they could originate from long-distance transport. It is very likely that they are equilibrated in larger gas-phase concentrations as SOA also increases with the elevation of $PM_{2.5}$ (Fig. S15). Whereas for $C_{11-14}H_{22-28}O_7N_2$, they are less volatile and lie in the range of low-volatility organic compounds, hence, they can hardly be transported and are more likely produced during the air mass transportation. Those pollution-related OOMs take the largest (14 %) and smallest (2 %) fraction in winter and summer respectively (Table S11). In terms of carbon distribution, there is not too much difference among seasons, in which the relatively short C4 to C9 aliphatic OOMs make up 83-90 % and the longer ones take up 10-17 % (Fig. S13).
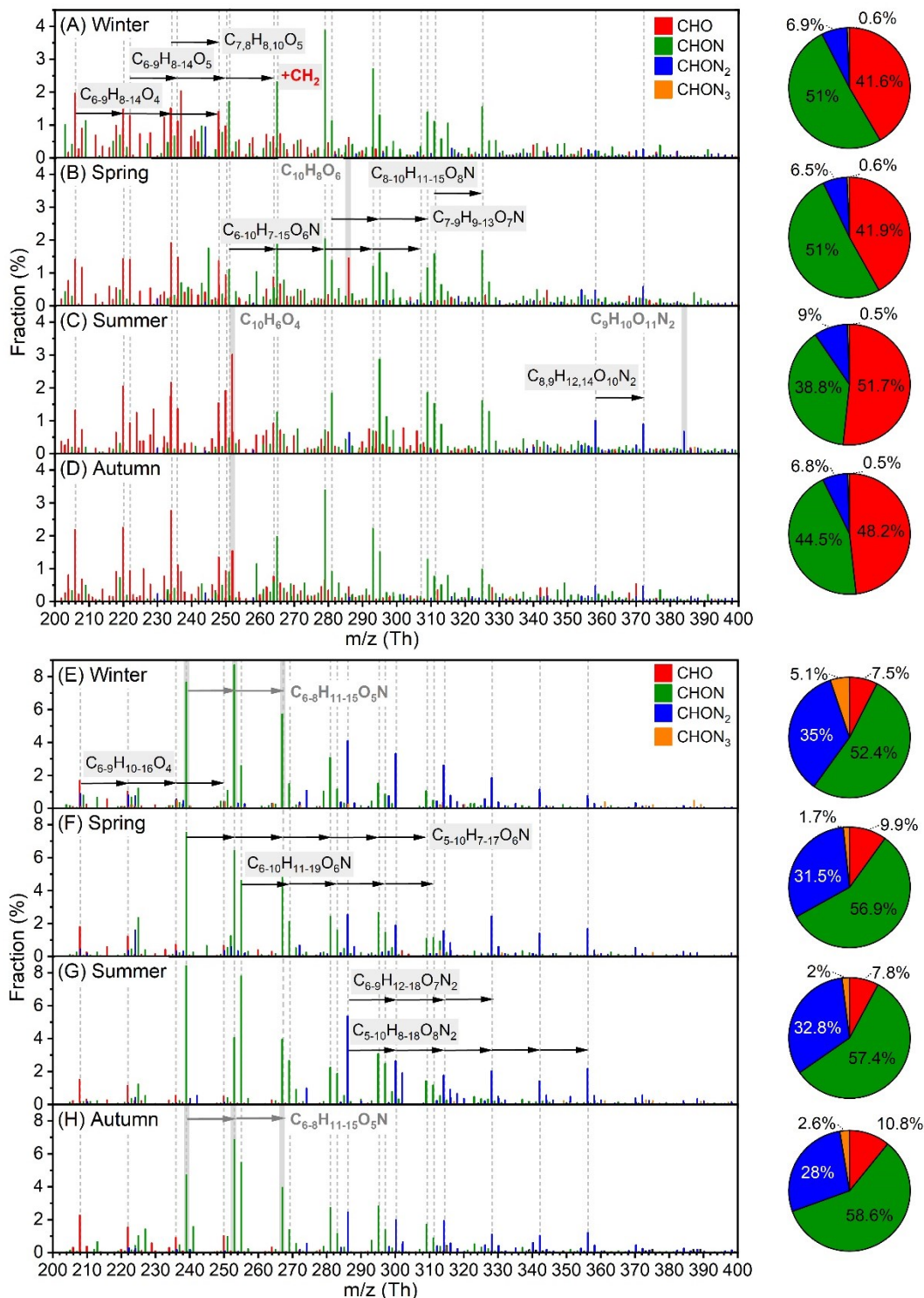
Figure 9. Fractional profiles of each aromatic OOM molecule in (A) winter, (B) spring, (C) summer and (D) autumn, and of each aliphatic OOM molecule in (E) winter, (F) spring, (G) summer and (H) autumn. The mass to charge ratio (m/z) denotes OOM clustered with NO_3^- or as deprotonated ones. The fraction of each compound is calculated as the ratio of its concentration to the total concentration of aromatic OOMs ((A) to (D)) or aliphatic OOMs ((E) to (H)). The red, green, blue and orange bars are for CHO, CHON, $CHON_2$ and $CHON_3$ OOMs respectively. Species marked with grey dashed lines are primary ones during the year, and species in grey background are special ones for specific seasons.

436   Up till now, field measurements of anthropogenic OOMs are rare (Nie et al., 2022;Liu et al., 2021). In general,
437   the concentrations of aromatic and aliphatic OOMs in Beijing are comparable with those in other Chinese
438   megacities (Table S13), and fingerprint aromatic and aliphatic OOM molecules in Beijing and Nanjing are also
439   identical (Table S14). This suggests that the OOM production, including both the precursor emissions and oxidation
440   mechanisms, may share high similarities in megacities. Yet, a more systematic comparison can only be made when
441   measurements at more locations are available in the future.
442

3.3. Atmospheric implication: OOM contribution to SOA through condensation

444   The volatility of organic compound determines its partitioning between gas and particle phases, and thus
445   influences its atmospheric lifetime, gas-phase concentration, and contribution to SOA. Therefore, we estimate the
446   volatility of source-classified OOMs (detailed method can be found in Sect. S3) and summarize the results in Fig.
447   10. The seasonal variations of OOMs classified as ELVOCs (extremely low-volatility organic compounds), LVOCs
448   (low-volatility organic compounds) and SVOCs (semi-volatile organic compounds) follow the same trend as that
449   of total OOMs, with the highest concentrations in summer (1.3×10^7 cm^{-3}, 4.0×10^7 cm^{-3} and 8.4×10^7 cm^{-3} for
450   ELVOCs, LVOCs, and SVOCs, respectively) and the lowest ones in winter (4.4×10^6 cm^{-3}, 9.4×10^6 cm^{-3} and 5.3×10^6
451   cm^{-3} for ELVOCs, LVOCs, and SVOCs, respectively). Here, we focus particularly on OOMs with relatively low
452   volatility with high potential contributing to the formation of SOA.

453   Due to the concentration variation of four source-classified OOMs and their temperature-dependent volatility
454   distribution (Table S16), their fractions within different volatility ranges have distinct seasonal characteristics (Fig.
455   10 (B)). Among ELVOCs, aromatic OOMs take the largest fractions, ranging from 72 to 94 % throughout the year.
456   For LVOCs, aromatic (34-51 %) and aliphatic OOMs (17-42 %) are the two that have the largest proportions. And
457   MT OOMs, favored by its low volatility (Table S16) (Tröstl et al., 2016;Yan et al., 2020), also take up ~ 14 % of
458   LVOCs in seasons other than winter. IP OOMs, however, due to its high volatility (Table S16) (Krechmer et al.,
459   2015;Xu et al., 2021), do not have an appreciable contribution to ELVOCs and LVOCs even in summer when its
460   concentration is exceedingly high. Consequently, it is likely that the pure condensation of IP OOMs has a minor
461   contribution to SOA growth regardless of the season.
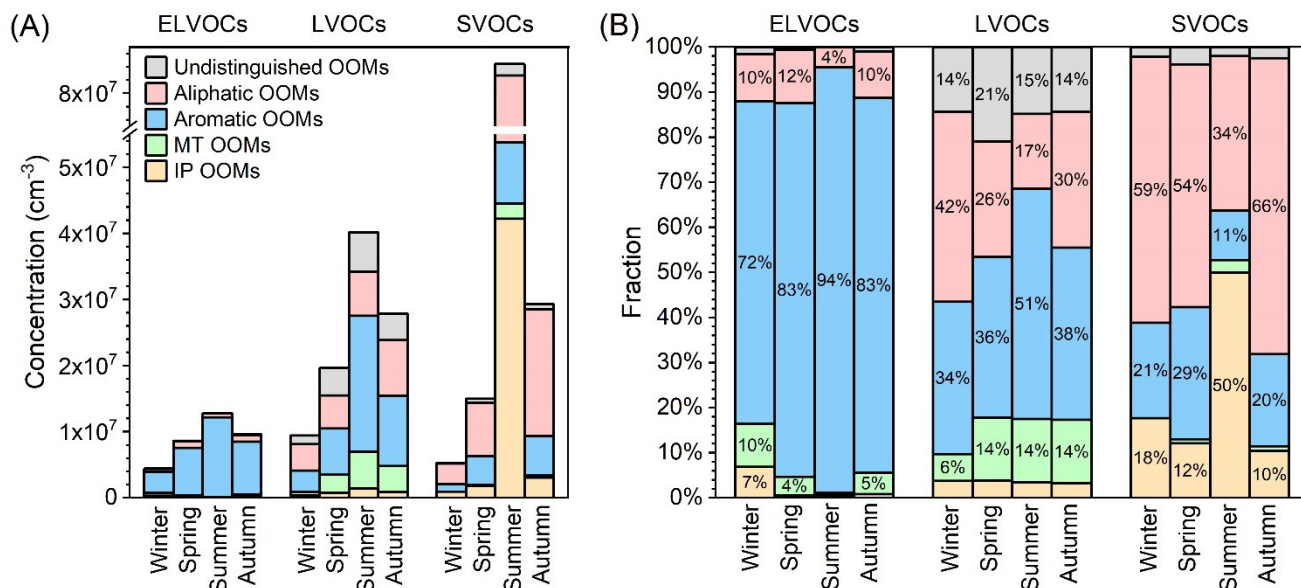
Figure 10. (A) Concentration and (B) fraction of source-classified OOMs in ELVOCs (extremely low volatile organic compounds), LVOCs (low volatile organic compounds) and SVOCs (semi-volatile organic compounds) in four seasons. Please also note that the fractions smaller than 4% are not marked.

The rate of OOM condensation onto particles, referred to as condensation flux hereafter, was calculated based on the particle dynamic model proposed by Trostl et al. (Tröstl et al., 2016) (see details in Sect. S5). In terms of seasonal variation (Fig. 11 (A)), OOM condensation flux exhibits the highest level in autumn (0.64 $\mu g \cdot m^{-3} \cdot h^{-1}$), followed by summer (0.61 $\mu g \cdot m^{-3} \cdot h^{-1}$), spring (0.41 $\mu g \cdot m^{-3} \cdot h^{-1}$), and decreases to the lowest in winter (0.30 $\mu g \cdot m^{-3} \cdot h^{-1}$). For seasonal comparison of SOA formation rate caused by OOM condensation, the characteristic accumulation time (AccTime), defined as SOA divided by OOM condensation flux, is calculated as an indicator (see details in Sect. S4). As shown in Fig. 11 (B), a characteristic time of 24 hours is enough to explain the observed SOA concentration by OOM condensation in winter, and it is reduced to 7 hours, 10 hours, and 7 hours for spring, summer, and autumn, respectively. It should be noted that this should not be interpreted as the entire SOA being formed via OOM condensation during this characteristic time, but rather that OOM condensation is efficient and can have a significant contribution to SOA formation. A recent study (Nie et al., 2022) suggested that OOM condensation can account for about 40% of the SOA formation in wintertime Beijing. Our analysis on seasonal variation indicates that the condensation of OOMs could have a larger contribution to SOA formation in seasons other than winter.

For OOMs from different sources, aromatic OOMs contributes the most during the year, varying from 46 % to 62 %, followed by aliphatic OOMs (14-32 %). In comparison, the two biogenic ones, MT OOMs (8-12 %) and IP OOMs (3-5 %), have smaller contribution in all the four seasons. This indicates that the formation of SOA through condensation in urban Beijing is dominated by anthropogenic sources, which is in line with the previously reported SOA composition (Le Breton et al., 2018;Mehra et al., 2021). Overall, our results suggest that in order to control the formation of SOA, the emission of anthropogenic VOCs, especially aromatics, should be restricted with a high priority.
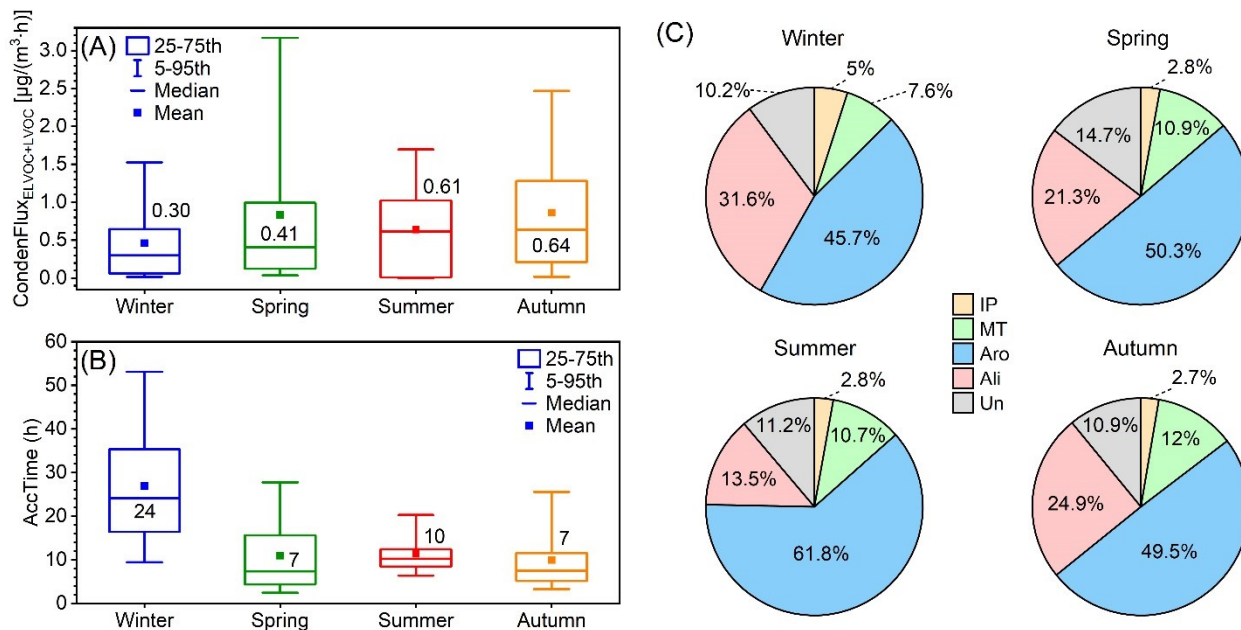
Figure 11. (A) Condensation flux of OOMs calculated by the particle dynamic model by Trostl et al. (Tröstl et al., 2016) in four seasons. (B) Characteristic accumulation time of SOA (AccTime), calculated as SOA divided by OOM condensation flux, in four season. This parameter is used as indicator for the relative accumulation rate of SOA caused by OOM condensation in different seasons. The values in each box of (A) and (B) are the median values of corresponding parameters. (C) Estimated condensation flux contribution of four source-classified OOMs in four seasons. The abbreviations "IP" "MT" "Aro" "Ali" and "Un" stand for IP OOMs, MT OOMs, aromatic OOMs, aliphatic OOMs and undistinguished OOMs respectively.

4. Summary and Conclusions

A long-term measurement of OOMs based on nitrate CIMS was conducted in urban Beijing. OOMs in the mass range of 200-400 Th were systematically investigated. Total OOM concentration in Beijing shows a clear dependence on UVB and temperature, suggesting the importance of photo-oxidation and temperature on OOM formation. In comparison to other atmospheric sites, total OOM concentration in Beijing (2.3×10^7 - 1.6×10^8 cm^{-3}) is generally comparable to urban and suburban areas, and is clearly lower than those measured in forested areas. In the case of composition, most OOMs have 5 to 10 carbon atoms, 3 to 7 effective oxygen atoms, 0 to 2 nitrogen atoms and 0 to 6 DBE values. The seasonal variation of average effective oxygen atom follows the same trend as the overall atmospheric oxidation capacity, being the highest in summer and the lowest in winter and autumn. While for nitrogen and DBE distribution, there are not too much difference among seasons disregarding isoprene OOMs, indicating that the dominant formation pathways of each source-classified OOMs stay constant during the year.

With a revised workflow, we further separate OOMs into isoprene, monoterpene, aromatic, and aliphatic OOMs. For relative abundance, aromatic (29-41 %) and aliphatic OOMs (26-41 %) are major contributors throughout the year, suggesting that OOMs in urban atmospheric environment are controlled by anthropogenic activities. In addition, isoprene OOMs play an important role in summer and their fraction reaches to 33 %, indicating that biogenic sources are also large contributors to total OOMs in warmer seasons. The concentration of isoprene OOMs

509 (0.2-5.3×10^7 cm^{-3}) and monoterpene OOMs (1.1-8.4×10^6 cm^{-3}) are smaller than those in forest areas, and they

510 exhibit higher nitrogen and lower oxygen content compared with other cleaner sites. One recent study (Nie et al.,

511 2022) reported that the composition of wintertime OOMs among four Chinese megacities, including Beijing, were

512 similar. Our study further demonstrates that the composition of summertime OOMs between Beijing and Nanjing

513 also have strong resemblance. Consequently, the seasonal characteristics of Beijing OOMs in this study could be

514 representative of OOMs in other Chinese metropolises.

515   In terms of volatility, monoterpene OOMs are the most condensable, isoprene OOMs are the most volatile, and

516 aromatic OOMs are more condensable than aliphatic ones. Based on the volatility and concentration characteristics

517 of the four source-classified OOMs, an aerosol growth model was utilized to calculate their contribution to SOA

518 growth. Results show that the condensation flux of total OOMs (0.30-0.64 μg·m^{-3}·h^{-1}) are high enough to produce

519 a considerable amount of SOA within a day, and that aromatic (46-62 %) and aliphatic (14-32 %) OOMs are found

520 to be dominant contributors regardless of seasons. This suggests that the formation of SOA in urban cities are likely

521 driven by OOMs from anthropogenic sources, and highlights the importance of reducing anthropogenic emissions,

522 especially aromatics, for pollution mitigation.

523

References

Aalto, P., Hämeri, K., Becker, E., Weber, R., Salm, J., Mäkelä, J. M., Hoell, C., O'dowd, C. D., Hansson, H.-C., Väkevä, M., Koponen, I. K., Buzorius, G., and Kulmala, M.: Physical characterization of aerosol particles during nucleation events, Tellus B: Chemical and Physical Meteorology, 53, 344-358, 10.3402/tellusb.v53i4.17127, 2001.

Berndt, T., Richters, S., Jokinen, T., Hyttinen, N., Kurtén, T., Otkjær, R. V., Kjaergaard, H. G., Stratmann, F., Herrmann, H., Sipilä, M., Kulmala, M., and Ehn, M.: Hydroxyl radical-induced formation of highly oxidized organic compounds, Nature Communications, 7, 13677, 10.1038/ncomms13677, 2016.

Berndt, T., Mentler, B., Scholz, W., Fischer, L., Herrmann, H., Kulmala, M., and Hansel, A.: Accretion Product Formation from Ozonolysis and OH Radical Reaction of α-Pinene: Mechanistic Insight and the Influence of Isoprene and Ethylene, Environmental Science & Technology, 52, 10.1021/acs.est.8b02210, 2018.

Bianchi, F., Tröstl, J., Junninen, H., Frege, C., Henne, S., Hoyle, C. R., Molteni, U., Herrmann, E., Adamov, A., Bukowiecki, N., Chen, X., Duplissy, J., Gysel, M., Hutterli, M., Kangasluoma, J., Kontkanen, J., Kürten, A., Manninen, H. E., Münch, S., Peräkylä, O., Petäjä, T., Rondo, L., Williamson, C., Weingartner, E., Curtius, J., Worsnop, D. R., Kulmala, M., Dommen, J., and Baltensperger, U.: New particle formation in the free troposphere: A question of chemistry and timing, Science, 352, 1109-1112, 10.1126/science.aad5456, 2016.

Bianchi, F., Garmash, O., He, X., Yan, C., Iyer, S., Rosendahl, I., Xu, Z., Rissanen, M. P., Riva, M., Taipale, R., Sarnela, N., Petäjä, T., Worsnop, D. R., Kulmala, M., Ehn, M., and Junninen, H.: The role of highly oxygenated molecules (HOMs) in determining the composition of ambient ions in the boreal forest, Atmos. Chem. Phys., 17, 13819-13831, 10.5194/acp-17-13819-2017, 2017.

Bianchi, F., Kurten, T., Riva, M., Mohr, C., Rissanen, M. P., Roldin, P., Berndt, T., Crounse, J. D., Wennberg, P. O., Mentel, T. F., Wildt, J., Junninen, H., Jokinen, T., Kulmala, M., Worsnop, D. R., Thornton, J. A., Donahue, N., Kjaergaard, H. G., and Ehn, M.: Highly Oxygenated Organic Molecules (HOM) from Gas-Phase Autoxidation Involving Peroxy Radicals: A Key Contributor to Atmospheric Aerosol, Chemical Reviews, 119, 3472-3509, 10.1021/acs.chemrev.8b00395, 2019.

Boyd, C. M., Sanchez, J., Xu, L., Eugene, A. J., Nah, T., Tuet, W. Y., Guzman, M. I., and Ng, N. L.: Secondary organic aerosol formation from the β-pinene+NO₃ system: effect of humidity and peroxy radical fate, Atmos. Chem. Phys., 15, 7497-7522, 10.5194/acp-15-7497-2015, 2015.

Brean, J., Harrison, R. M., Shi, Z., Beddows, D. C. S., Acton, W. J. F., Hewitt, C. N., Squires, F. A., and Lee, J.: Observations of highly oxidized molecules and particle nucleation in the atmosphere of Beijing, Atmos. Chem. Phys., 19, 14933-14947, 10.5194/acp-19-14933-2019, 2019.

Caudillo, L., Rörup, B., Heinritzi, M., Marie, G., Simon, M., Wagner, A. C., Müller, T., Granzin, M., Amorim, A., Ataei, F., Baalbaki, R., Bertozzi, B., Brasseur, Z., Chiu, R., Chu, B., Dada, L., Duplissy, J., Finkenzeller, H., Gonzalez Carracedo, L., He, X. C., Hofbauer, V., Kong, W., Lamkaddam, H., Lee, C. P., Lopez, B., Mahfouz, N. G. A., Makhmutov, V., Manninen, H. E., Marten, R., Massabò, D., Mauldin, R. L., Mentler, B., Molteni, U., Onnela, A., Pfeifer, J., Philippov, M., Piedehierro, A. A., Schervish, M., Scholz, W., Schulze, B., Shen, J., Stolzenburg, D., Stozhkov, Y., Surdu, M., Tauber, C., Tham, Y. J., Tian, P., Tomé, A., Vogt, S., Wang, M., Wang, D. S., Weber, S. K., Welti, A., Yonghong, W., Yusheng, W., Zauner-Wieczorek, M., Baltensperger, U., El Haddad, I., Flagan, R. C., Hansel, A., Höhler, K., Kirkby, J., Kulmala, M., Lehtipalo, K., Möhler, O., Saathoff, H., Volkamer, R., Winkler, P. M., Donahue, N. M., Kürten, A., and Curtius, J.: Chemical composition of nanoparticles from α-pinene nucleation and the influence of isoprene and relative humidity at low temperature, Atmos. Chem. Phys. Discuss., 2021, 1-26, 10.5194/acp-2021-512, 2021.

580 Chen, D., Xia, L., Guo, X., Lang, J., Zhou, Y., Wei, L., and Fu, X.: Impact of inter-annual meteorological variation
581 from 2001 to 2015 on the contribution of regional transport to $PM_{2.5}$ in Beijing, China, Atmospheric Environment,
582 260, 118545, https://doi.org/10.1016/j.atmosenv.2021.118545, 2021.
583 Chen, D., Jin, X., Fu, X., Xia, L., Guo, X., Lang, J., Zhou, Y., and Wei, W.: Impact of Inter-Annual Variation in
584 Meteorology from 2010 to 2019 on the Inter-City Transport of $PM_{2.5}$ in the Beijing–Tianjin–Hebei
585 Region, Sustainability, 14, 10.3390/su14106210, 2022.
586 Cheng, X., Li, H., Zhang, Y., Li, Y., Zhang, W., Wang, X., Bi, F., Zhang, H., Gao, J., Chai, F., Lun, X., Chen, Y.,
587 Gao, J., and Lv, J.: Atmospheric isoprene and monoterpenes in a typical urban area of Beijing: Pollution
588 characterization, chemical reactivity and source identification, Journal of Environmental Sciences, 71, 150-167,
589 https://doi.org/10.1016/j.jes.2017.12.017, 2018.
590 Dada, L., Paasonen, P., Nieminen, T., Buenrostro Mazon, S., Kontkanen, J., Peräkylä, O., Lehtipalo, K., Hussein,
591 T., Petäjä, T., Kerminen, V. M., Bäck, J., and Kulmala, M.: Long-term analysis of clear-sky new particle formation
592 events and nonevents in Hyytiälä, Atmos. Chem. Phys., 17, 6227-6241, 10.5194/acp-17-6227-2017, 2017.
593 Donahue, N. M., Ortega, I. K., Chuang, W., Riipinen, I., Riccobono, F., Schobesberger, S., Dommen, J.,
594 Baltensperger, U., Kulmala, M., Worsnop, D. R., and Vehkamaki, H.: How do organic vapors contribute to new-
595 particle formation?, Faraday Discussions, 165, 91-104, 10.1039/C3FD00046J, 2013.
596 Drewnick, F., Hings, S. S., DeCarlo, P., Jayne, J. T., Gonin, M., Fuhrer, K., Weimer, S., Jimenez, J. L., Demerjian,
597 K. L., Borrmann, S., and Worsnop, D. R.: A New Time-of-Flight Aerosol Mass Spectrometer (TOF-AMS)—
598 Instrument Description and First Field Deployment, Aerosol Science and Technology, 39, 637-658,
599 10.1080/02786820500182040, 2005.
600 Ehn, M., Junninen, H., Petäjä, T., Kurtén, T., Kerminen, V. M., Schobesberger, S., Manninen, H. E., Ortega, I. K.,
601 Vehkamäki, H., Kulmala, M., and Worsnop, D. R.: Composition and temporal behavior of ambient ions in the
602 boreal forest, Atmos. Chem. Phys., 10, 8513-8530, 10.5194/acp-10-8513-2010, 2010.
603 Ehn, M., Kleist, E., Junninen, H., Petäjä, T., Lönn, G., Schobesberger, S., Dal Maso, M., Trimborn, A., Kulmala,
604 M., Worsnop, D. R., Wahner, A., Wildt, J., and Mentel, T. F.: Gas phase formation of extremely oxidized pinene
605 reaction products in chamber and ambient air, Atmos. Chem. Phys., 12, 5113-5127, 10.5194/acp-12-5113-2012,
606 2012.
607 Ehn, M., Thornton, J. A., Kleist, E., Sipilä, M., Junninen, H., Pullinen, I., Springer, M., Rubach, F., Tillmann, R.,
608 Lee, B., Lopez-Hilfiker, F., Andres, S., Acir, I.-H., Rissanen, M., Jokinen, T., Schobesberger, S., Kangasluoma, J.,
609 Kontkanen, J., Nieminen, T., Kurtén, T., Nielsen, L. B., Jørgensen, S., Kjaergaard, H. G., Canagaratna, M., Maso,
610 M. D., Berndt, T., Petäjä, T., Wahner, A., Kerminen, V.-M., Kulmala, M., Worsnop, D. R., Wildt, J., and Mentel,
611 T. F.: A large source of low-volatility secondary organic aerosol, Nature, 506, 476-479, 10.1038/nature13032, 2014.
612 Garmash, O., Rissanen, M. P., Pullinen, I., Schmitt, S., Kausiala, O., Tillmann, R., Zhao, D., Percival, C., Bannan,
613 T. J., Priestley, M., Hallquist, A. M., Kleist, E., Kiendler-Scharr, A., Hallquist, M., Berndt, T., McFiggans, G.,
614 Wildt, J., Mentel, T., and Ehn, M.: Multi-generation OH oxidation as a source for highly oxygenated organic
615 molecules from aromatics, Atmospheric Chemistry and Physics, 20, 515-537, 10.5194/acp-20-515-2020, 2020.
616 Gordon, H., Kirkby, J., Baltensperger, U., Bianchi, F., Breitenlechner, M., Curtius, J., Dias, A., Dommen, J.,
617 Donahue, N. M., Dunne, E. M., Duplissy, J., Ehrhart, S., Flagan, R. C., Frege, C., Fuchs, C., Hansel, A., Hoyle, C.
618 R., Kulmala, M., Kürten, A., Lehtipalo, K., Makhmutov, V., Molteni, U., Rissanen, M. P., Stozhkov, Y., Tröstl, J.,
619 Tsagkogeorgas, G., Wagner, R., Williamson, C., Wimmer, D., Winkler, P. M., Yan, C., and Carslaw, K. S.: Causes
620 and importance of new particle formation in the present-day and preindustrial atmospheres, Journal of Geophysical
621 Research: Atmospheres, 122, 8739-8760, https://doi.org/10.1002/2017JD026844, 2017.

Guo, Y., Yan, C., Li, C., Ma, W., Feng, Z., Zhou, Y., Lin, Z., Dada, L., Stolzenburg, D., Yin, R., Kontkanen, J., Daellenbach, K. R., Kangasluoma, J., Yao, L., Chu, B., Wang, Y., Cai, R., Bianchi, F., Liu, Y., and Kulmala, M.: Formation of nighttime sulfuric acid from the ozonolysis of alkenes in Beijing, Atmos. Chem. Phys., 21, 5499-5511, 10.5194/acp-21-5499-2021, 2021.

Hallquist, M., Wenger, J. C., Baltensperger, U., Rudich, Y., Simpson, D., Claeys, M., Dommen, J., Donahue, N. M., George, C., Goldstein, A. H., Hamilton, J. F., Herrmann, H., Hoffmann, T., Iinuma, Y., Jang, M., Jenkin, M. E., Jimenez, J. L., Kiendler-Scharr, A., Maenhaut, W., McFiggans, G., Mentel, T. F., Monod, A., Prevot, A. S. H., Seinfeld, J. H., Surratt, J. D., Szmigielski, R., and Wildt, J.: The formation, properties and impact of secondary organic aerosol: current and emerging issues, Atmospheric Chemistry and Physics, 9, 5155-5236, 10.5194/acp-9-5155-2009, 2009.

Heinritzi, M., Simon, M., Steiner, G., Wagner, A. C., Kürten, A., Hansel, A., and Curtius, J.: Characterization of the mass-dependent transmission efficiency of a CIMS, Atmos. Meas. Tech., 9, 1449-1460, 10.5194/amt-9-1449-2016, 2016.

Heinritzi, M., Dada, L., Simon, M., Stolzenburg, D., Wagner, A. C., Fischer, L., Ahonen, L. R., Amanatidis, S., Baalbaki, R., Baccarini, A., Bauer, P. S., Baumgartner, B., Bianchi, F., Brilke, S., Chen, D., Chiu, R., Dias, A., Dommen, J., Duplissy, J., Finkenzeller, H., Frege, C., Fuchs, C., Garmash, O., Gordon, H., Granzin, M., El Haddad, I., He, X., Helm, J., Hofbauer, V., Hoyle, C. R., Kangasluoma, J., Keber, T., Kim, C., Kürten, A., Lamkaddam, H., Laurila, T. M., Lampilahti, J., Lee, C. P., Lehtipalo, K., Leiminger, M., Mai, H., Makhmutov, V., Manninen, H. E., Marten, R., Mathot, S., Mauldin, R. L., Mentler, B., Molteni, U., Müller, T., Nie, W., Nieminen, T., Onnela, A., Partoll, E., Passananti, M., Petäjä, T., Pfeifer, J., Pospisilova, V., Quéléver, L. L. J., Rissanen, M. P., Rose, C., Schobesberger, S., Scholz, W., Scholze, K., Sipilä, M., Steiner, G., Stozhkov, Y., Tauber, C., Tham, Y. J., Vazquez-Pufleau, M., Virtanen, A., Vogel, A. L., Volkamer, R., Wagner, R., Wang, M., Weitz, L., Wimmer, D., Xiao, M., Yan, C., Ye, P., Zha, Q., Zhou, X., Amorim, A., Baltensperger, U., Hansel, A., Kulmala, M., Tomé, A., Winkler, P. M., Worsnop, D. R., Donahue, N. M., Kirkby, J., and Curtius, J.: Molecular understanding of the suppression of new-particle formation by isoprene, Atmos. Chem. Phys., 20, 11809-11821, 10.5194/acp-20-11809-2020, 2020.

Huang, W., Li, H., Sarnela, N., Heikkinen, L., Tham, Y. J., Mikkilä, J., Thomas, S. J., Donahue, N. M., Kulmala, M., and Bianchi, F.: Measurement report: Molecular composition and volatility of gaseous organic compounds in a boreal forest: from volatile organic compounds to highly oxygenated organic molecules, Atmos. Chem. Phys. Discuss., 2020, 1-27, 10.5194/acp-2020-1257, 2020.

Hyttinen, N., Kupiainen-Määttä, O., Rissanen, M. P., Muuronen, M., Ehn, M., and Kurtén, T.: Modeling the Charging of Highly Oxidized Cyclohexene Ozonolysis Products Using Nitrate-Based Chemical Ionization, The Journal of Physical Chemistry A, 119, 6339-6345, 10.1021/acs.jpca.5b01818, 2015.

Hyttinen, N., Otkjær, R. V., Iyer, S., Kjaergaard, H. G., Rissanen, M. P., Wennberg, P. O., and Kurtén, T.: Computational Comparison of Different Reagent Ions in the Chemical Ionization of Oxidized Multifunctional Compounds, The Journal of Physical Chemistry A, 122, 269-279, 10.1021/acs.jpca.7b10015, 2018.

Jayne, J. T., Leard, D. C., Zhang, X., Davidovits, P., Smith, K. A., Kolb, C. E., and Worsnop, D. R.: Development of an Aerosol Mass Spectrometer for Size and Composition Analysis of Submicron Particles, Aerosol Science and Technology, 33, 49-70, 10.1080/027868200410840, 2000.

Jimenez, J. L., Canagaratna, M. R., Donahue, N. M., Prevot, A. S. H., Zhang, Q., Kroll, J. H., DeCarlo, P. F., Allan, J. D., Coe, H., Ng, N. L., Aiken, A. C., Docherty, K. S., Ulbrich, I. M., Grieshop, A. P., Robinson, A. L., Duplissy, J., Smith, J. D., Wilson, K. R., Lanz, V. A., Hueglin, C., Sun, Y. L., Tian, J., Laaksonen, A., Raatikainen, T., Rautiainen, J., Vaattovaara, P., Ehn, M., Kulmala, M., Tomlinson, J. M., Collins, D. R., Cubison, M. J., Dunlea, J.,

Huffman, J. A., Onasch, T. B., Alfarra, M. R., Williams, P. I., Bower, K., Kondo, Y., Schneider, J., Drewnick, F., Borrmann, S., Weimer, S., Demerjian, K., Salcedo, D., Cottrell, L., Griffin, R., Takami, A., Miyoshi, T., Hatakeyama, S., Shimono, A., Sun, J. Y., Zhang, Y. M., Dzepina, K., Kimmel, J. R., Sueper, D., Jayne, J. T., Herndon, S. C., Trimborn, A. M., Williams, L. R., Wood, E. C., Middlebrook, A. M., Kolb, C. E., Baltensperger, U., and Worsnop, D. R.: Evolution of Organic Aerosols in the Atmosphere, Science, 326, 1525, 10.1126/science.1180353, 2009.

Jokinen, T., Sipilä, M., Junninen, H., Ehn, M., Lönn, G., Hakala, J., Petäjä, T., Mauldin Iii, R. L., Kulmala, M., and Worsnop, D. R.: Atmospheric sulphuric acid and neutral cluster measurements using CI-APi-TOF, Atmos. Chem. Phys., 12, 4117-4125, 10.5194/acp-12-4117-2012, 2012.

Jokinen, T., Sipilä, M., Richters, S., Kerminen, V.-M., Paasonen, P., Stratmann, F., Worsnop, D., Kulmala, M., Ehn, M., Herrmann, H., and Berndt, T.: Rapid Autoxidation Forms Highly Oxidized RO_2 Radicals in the Atmosphere, Angewandte Chemie International Edition, 53, 14596-14600, https://doi.org/10.1002/anie.201408566, 2014.

Junninen, H., Ehn, M., Petäjä, T., Luosujärvi, L., Kotiaho, T., Kostiainen, R., Rohner, U., Gonin, M., Fuhrer, K., Kulmala, M., and Worsnop, D. R.: A high-resolution mass spectrometer to measure atmospheric ion composition, Atmos. Meas. Tech., 3, 1039-1053, 10.5194/amt-3-1039-2010, 2010.

Kirkby, J., Duplissy, J., Sengupta, K., Frege, C., Gordon, H., Williamson, C., Heinritzi, M., Simon, M., Yan, C., Almeida, J., Tröstl, J., Nieminen, T., Ortega, I. K., Wagner, R., Adamov, A., Amorim, A., Bernhammer, A.-K., Bianchi, F., Breitenlechner, M., Brilke, S., Chen, X., Craven, J., Dias, A., Ehrhart, S., Flagan, R. C., Franchin, A., Fuchs, C., Guida, R., Hakala, J., Hoyle, C. R., Jokinen, T., Junninen, H., Kangasluoma, J., Kim, J., Krapf, M., Kürten, A., Laaksonen, A., Lehtipalo, K., Makhmutov, V., Mathot, S., Molteni, U., Onnela, A., Peräkylä, O., Piel, F., Petäjä, T., Praplan, A. P., Pringle, K., Rap, A., Richards, N. A. D., Riipinen, I., Rissanen, M. P., Rondo, L., Sarnela, N., Schobesberger, S., Scott, C. E., Seinfeld, J. H., Sipilä, M., Steiner, G., Stozhkov, Y., Stratmann, F., Tomé, A., Virtanen, A., Vogel, A. L., Wagner, A. C., Wagner, P. E., Weingartner, E., Wimmer, D., Winkler, P. M., Ye, P., Zhang, X., Hansel, A., Dommen, J., Donahue, N. M., Worsnop, D. R., Baltensperger, U., Kulmala, M., Carslaw, K. S., and Curtius, J.: Ion-induced nucleation of pure biogenic particles, Nature, 533, 521-526, 10.1038/nature17953, 2016.

Krechmer, J. E., Coggon, M. M., Massoli, P., Nguyen, T. B., Crounse, J. D., Hu, W., Day, D. A., Tyndall, G. S., Henze, D. K., Rivera-Rios, J. C., Nowak, J. B., Kimmel, J. R., Mauldin, R. L., Stark, H., Jayne, J. T., Sipilä, M., Junninen, H., St. Clair, J. M., Zhang, X., Feiner, P. A., Zhang, L., Miller, D. O., Brune, W. H., Keutsch, F. N., Wennberg, P. O., Seinfeld, J. H., Worsnop, D. R., Jimenez, J. L., and Canagaratna, M. R.: Formation of Low Volatility Organic Compounds and Secondary Organic Aerosol from Isoprene Hydroxyhydroperoxide Low-NO Oxidation, Environmental Science & Technology, 49, 10330-10339, 10.1021/acs.est.5b02031, 2015.

Kulmala, M., Kontkanen, J., Junninen, H., Lehtipalo, K., Manninen, H. E., Nieminen, T., Petäjä, T., Sipilä, M., Schobesberger, S., Rantala, P., Franchin, A., Jokinen, T., Järvinen, E., Äijälä, M., Kangasluoma, J., Hakala, J., Aalto, P. P., Paasonen, P., Mikkilä, J., Vanhanen, J., Aalto, J., Hakola, H., Makkonen, U., Ruuskanen, T., Mauldin, R. L., 3rd, Duplissy, J., Vehkamäki, H., Bäck, J., Kortelainen, A., Riipinen, I., Kurtén, T., Johnston, M. V., Smith, J. N., Ehn, M., Mentel, T. F., Lehtinen, K. E., Laaksonen, A., Kerminen, V. M., and Worsnop, D. R.: Direct observations of atmospheric aerosol nucleation, Science, 339, 943-946, 10.1126/science.1227385, 2013.

Kürten, A., Bergen, A., Heinritzi, M., Leiminger, M., Lorenz, V., Piel, F., Simon, M., Sitals, R., Wagner, A. C., and Curtius, J.: Observation of new particle formation and measurement of sulfuric acid, ammonia, amines and highly oxidized organic molecules at a rural site in central Germany, Atmos. Chem. Phys., 16, 12793-12813, 10.5194/acp-16-12793-2016, 2016.

706 Le Breton, M., Wang, Y., Hallquist, Å. M., Pathak, R. K., Zheng, J., Yang, Y., Shang, D., Glasius, M., Bannan, T.
707 J., Liu, Q., Chan, C. K., Percival, C. J., Zhu, W., Lou, S., Topping, D., Wang, Y., Yu, J., Lu, K., Guo, S., Hu, M.,
708 and Hallquist, M.: Online gas- and particle-phase measurements of organosulfates, organosulfonates and nitrooxy
709 organosulfates in Beijing utilizing a FIGAERO ToF-CIMS, Atmos. Chem. Phys., 18, 10355-10371, 10.5194/acp-
710 18-10355-2018, 2018.

711 Lehtipalo, K., Yan, C., Dada, L., Bianchi, F., Xiao, M., Wagner, R., Stolzenburg, D., Ahonen, L., Amorim, A.,
712 Baccarini, A., Bauer, P., Baumgartner, B., Bergen, A., Bernhammer, A.-K., Breitenlechner, M., Brilke, S., Buchholz,
713 A., Mazon, S., Chen, D., and Worsnop, D.: Multicomponent new particle formation from sulfuric acid, ammonia,
714 and biogenic vapors, Science Advances, 4, eaau5363, 10.1126/sciadv.aau5363, 2018.

715 Lelieveld, J., Evans, J. S., Fnais, M., Giannadaki, D., and Pozzer, A.: The contribution of outdoor air pollution
716 sources to premature mortality on a global scale, Nature, 525, 367-371, 10.1038/nature15371, 2015.

717 Liu, Y., Yan, C., Feng, Z., Zheng, F., Fan, X., Zhang, Y., Li, C., Zhou, Y., Lin, Z., Guo, Y., Zhang, Y., Ma, L.,
718 Zhou, W., Liu, Z., Dada, L., Dällenbach, K., Kontkanen, J., Cai, R., Chan, T., Chu, B., Du, W., Yao, L., Wang, Y.,
719 Cai, J., Kangasluoma, J., Kokkonen, T., Kujansuu, J., Rusanen, A., Deng, C., Fu, Y., Yin, R., Li, X., Lu, Y., Liu,
720 Y., Lian, C., Yang, D., Wang, W., Ge, M., Wang, Y., Worsnop, D. R., Junninen, H., He, H., Kerminen, V.-M.,
721 Zheng, J., Wang, L., Jiang, J., Petäjä, T., Bianchi, F., and Kulmala, M.: Continuous and comprehensive atmospheric
722 observations in Beijing: a station to understand the complex urban atmospheric environment, Big Earth Data, 4,
723 295-321, 10.1080/20964471.2020.1798707, 2020.

724 Liu, Y., Nie, W., Li, Y., Ge, D., Liu, C., Xu, Z., Chen, L., Wang, T., Wang, L., Sun, P., Qi, X., Wang, J., Xu, Z.,
725 Yuan, J., Yan, C., Zhang, Y., Huang, D., Wang, Z., Donahue, N. M., Worsnop, D., Chi, X., Ehn, M., and Ding, A.:
726 Formation of condensable organic vapors from anthropogenic and biogenic volatile organic compounds (VOCs) is
727 strongly perturbed by NOx in eastern China, Atmos. Chem. Phys., 21, 14789-14814, 10.5194/acp-21-14789-2021,
728 2021.

729 Massoli, P., Stark, H., Canagaratna, M. R., Krechmer, J. E., Xu, L., Ng, N. L., Mauldin, R. L., Yan, C., Kimmel, J.,
730 Misztal, P. K., Jimenez, J. L., Jayne, J. T., and Worsnop, D. R.: Ambient Measurements of Highly Oxidized Gas-
731 Phase Molecules during the Southern Oxidant and Aerosol Study (SOAS) 2013, ACS Earth and Space Chemistry,
732 2, 653-672, 10.1021/acsearthspacechem.8b00028, 2018.

733 Mehra, A., Canagaratna, M., Bannan, T. J., Worrall, S. D., Bacak, A., Priestley, M., Liu, D., Zhao, J., Xu, W., Sun,
734 Y., Hamilton, J. F., Squires, F. A., Lee, J., Bryant, D. J., Hopkins, J. R., Elzein, A., Budisulistiorini, S. H., Cheng,
735 X., Chen, Q., Wang, Y., Wang, L., Stark, H., Krechmer, J. E., Brean, J., Slater, E., Whalley, L., Heard, D., Ouyang,
736 B., Acton, W. J. F., Hewitt, C. N., Wang, X., Fu, P., Jayne, J., Worsnop, D., Allan, J., Percival, C., and Coe, H.:
737 Using highly time-resolved online mass spectrometry to examine biogenic and anthropogenic contributions to
738 organic aerosol in Beijing, Faraday Discussions, 10.1039/D0FD00080A, 2021.

739 Merikanto, J., Spracklen, D. V., Mann, G. W., Pickering, S. J., and Carslaw, K. S.: Impact of nucleation on global
740 CCN, Atmos. Chem. Phys., 9, 8601-8616, 10.5194/acp-9-8601-2009, 2009.

741 Mo, Z., Shao, M., Wang, W., Liu, Y., Wang, M., and Lu, S.: Evaluation of biogenic isoprene emissions and their
742 contribution to ozone formation by ground-based measurements in Beijing, China, Science of The Total
743 Environment, 627, 1485-1494, https://doi.org/10.1016/j.scitotenv.2018.01.336, 2018.

744 Mohr, C., Thornton, J. A., Heitto, A., Lopez-Hilfiker, F. D., Lutz, A., Riipinen, I., Hong, J., Donahue, N. M.,
745 Hallquist, M., Petäjä, T., Kulmala, M., and Yli-Juuti, T.: Molecular identification of organic vapors driving
746 atmospheric nanoparticle growth, Nature Communications, 10, 4442, 10.1038/s41467-019-12473-2, 2019.

747 Molteni, U., Bianchi, F., Klein, F., El Haddad, I., Frege, C., Rossi, M. J., Dommen, J., and Baltensperger, U.:
748 Formation of highly oxygenated organic molecules from aromatic compounds, Atmos. Chem. Phys., 18, 1909-1921,
749 10.5194/acp-18-1909-2018, 2018.

750 Mutzel, A., Poulain, L., Berndt, T., Iinuma, Y., Rodigast, M., Böge, O., Richters, S., Spindler, G., Sipilä, M.,
751 Jokinen, T., Kulmala, M., and Herrmann, H.: Highly Oxidized Multifunctional Organic Compounds Observed in
752 Tropospheric Particles: A Field and Laboratory Study, Environmental Science & Technology, 49, 7754-7761,
753 10.1021/acs.est.5b00885, 2015.

754 Nah, T., Sanchez, J., Boyd, C., and Ng, N.: Photochemical Aging of α-pinene and β-pinene Secondary Organic
755 Aerosol formed from Nitrate Radical Oxidation, Environmental Science & Technology, 50,
756 10.1021/acs.est.5b04594, 2015.

757 Nie, W., Yan, C., Huang, D. D., Wang, Z., Liu, Y., Qiao, X., Guo, Y., Tian, L., Zheng, P., Xu, Z., Li, Y., Xu, Z.,
758 Qi, X., Sun, P., Wang, J., Zheng, F., Li, X., Yin, R., Dallenbach, K. R., Bianchi, F., Petäjä, T., Zhang, Y., Wang,
759 M., Schervish, M., Wang, S., Qiao, L., Wang, Q., Zhou, M., Wang, H., Yu, C., Yao, D., Guo, H., Ye, P., Lee, S.,
760 Li, Y. J., Liu, Y., Chi, X., Kerminen, V.-M., Ehn, M., Donahue, N. M., Wang, T., Huang, C., Kulmala, M., Worsnop,
761 D., Jiang, J., and Ding, A.: Secondary organic aerosol formed by condensing anthropogenic vapours over China's
762 megacities, Nature Geoscience, 15, 255-261, 10.1038/s41561-022-00922-5, 2022.

763 O'Dowd, C. D., Aalto, P., Hmeri, K., Kulmala, M., and Hoffmann, T.: Atmospheric particles from organic vapours,
764 Nature, 416, 497-498, 10.1038/416497a, 2002.

765 Orlando, J. J., and Tyndall, G. S.: Laboratory studies of organic peroxy radical chemistry: an overview with
766 emphasis on recent issues of atmospheric significance, Chemical Society Reviews, 41, 6294-6317,
767 10.1039/C2CS35166H, 2012.

768 Pan, S., and Wang, L.: Atmospheric Oxidation Mechanism of m-Xylene Initiated by OH Radical, The Journal of
769 Physical Chemistry A, 118, 10778-10787, 10.1021/jp506815v, 2014.

770 Panopoulou, A., Liakakou, E., Sauvage, S., Gros, V., Locoge, N., Stavroulas, I., Bonsang, B., Gerasopoulos, E.,
771 and Mihalopoulos, N.: Yearlong measurements of monoterpenes and isoprene in a Mediterranean city (Athens):
772 Natural vs anthropogenic origin, Atmospheric Environment, 243, 117803,
773 https://doi.org/10.1016/j.atmosenv.2020.117803, 2020.

774 Riccobono, F., Schobesberger, S., Scott, C., Dommen, J., Ortega, I., Rondo, L., Almeida, J., Amorim, A., Bianchi,
775 F., Breitenlechner, M., David, A., Downard, A., Dunne, E., Duplissy, J., Ehrhart, S., Flagan, R., Franchin, A.,
776 Hansel, A., Junninen, H., and Baltensperger, U.: Oxidation Products of Biogenic Emissions Contribute to
777 Nucleation of Atmospheric Particles, Science (New York, N.Y.), 344, 717-721, 10.1126/science.1243527, 2014.

778 Riedel, T. P., Lin, Y.-H., Budisulistiorini, S. H., Gaston, C. J., Thornton, J. A., Zhang, Z., Vizuete, W., Gold, A.,
779 and Surratt, J. D.: Heterogeneous Reactions of Isoprene-Derived Epoxides: Reaction Probabilities and Molar
780 Secondary Organic Aerosol Yield Estimates, Environmental Science & Technology Letters, 2, 38-42,
781 10.1021/ez500406f, 2015.

782 Riva, M., Rantala, P., Krechmer, J. E., Peräkylä, O., Zhang, Y., Heikkinen, L., Garmash, O., Yan, C., Kulmala, M.,
783 Worsnop, D., and Ehn, M.: Evaluating the performance of five different chemical ionization techniques for
784 detecting gaseous oxygenated organic species, Atmos. Meas. Tech., 12, 2403-2421, 10.5194/amt-12-2403-2019,
785 2019.

786 Roldin, P., Ehn, M., Kurtén, T., Olenius, T., Rissanen, M. P., Sarnela, N., Elm, J., Rantala, P., Hao, L., Hyttinen,
787 N., Heikkinen, L., Worsnop, D. R., Pichelstorfer, L., Xavier, C., Clusius, P., Öström, E., Petäjä, T., Kulmala, M.,

788 Vehkamäki, H., Virtanen, A., Riipinen, I., and Boy, M.: The role of highly oxygenated organic molecules in the
789 Boreal aerosol-cloud-climate system, Nature Communications, 10, 4370, 10.1038/s41467-019-12338-8, 2019.
790 Rose, C., Zha, Q., Dada, L., Yan, C., Lehtipalo, K., Junninen, H., Mazon, S. B., Jokinen, T., Sarnela, N., Sipilä, M.,
791 Petäjä, T., Kerminen, V.-M., Bianchi, F., and Kulmala, M.: Observations of biogenic ion-induced cluster formation
792 in the atmosphere, Science Advances, 4, eaar5218, 10.1126/sciadv.aar5218, 2018.
793 Schervish, M., and Donahue, N. M.: Peroxy radical chemistry and the volatility basis set, Atmos. Chem. Phys., 20,
794 1183-1199, 10.5194/acp-20-1183-2020, 2020.
795 Schobesberger, S., Junninen, H., Bianchi, F., Lönn, G., Ehn, M., Lehtipalo, K., Dommen, J., Ehrhart, S., Ortega, I.
796 K., Franchin, A., Nieminen, T., Riccobono, F., Hutterli, M., Duplissy, J., Almeida, J., Amorim, A., Breitenlechner,
797 M., Downard, A. J., Dunne, E. M., Flagan, R. C., Kajos, M., Keskinen, H., Kirkby, J., Kupc, A., Kürten, A., Kurtén,
798 T., Laaksonen, A., Mathot, S., Onnela, A., Praplan, A. P., Rondo, L., Santos, F. D., Schallhart, S., Schnitzhofer, R.,
799 Sipilä, M., Tomé, A., Tsagkogeorgas, G., Vehkamäki, H., Wimmer, D., Baltensperger, U., Carslaw, K. S., Curtius,
800 J., Hansel, A., Petäjä, T., Kulmala, M., Donahue, N. M., and Worsnop, D. R.: Molecular understanding of
801 atmospheric particle formation from sulfuric acid and large oxidized organic molecules, Proceedings of the National
802 Academy of Sciences, 110, 17223, 10.1073/pnas.1306973110, 2013.
803 Seinfeld, J. H., and Pandis, S. N.: Atmospheric chemistry and physics: from air pollution to climate change, John
804 Wiley & Sons, 2016.
805 Song, K., Guo, S., Wang, H., Yu, Y., Wang, H., Tang, R., Xia, S., Gong, Y., Wan, Z., Lv, D., Tan, R., Zhu, W.,
806 Shen, R., Li, X., Yu, X., Chen, S., Zeng, L., and Huang, X.: Measurement Report: Online Measurement of Gas-
807 Phase Nitrated Phenols Utilizing CI-LToF-MS: Primary Sources and Secondary Formation, Atmos. Chem. Phys.
808 Discuss., 2021, 1-28, 10.5194/acp-2020-1294, 2021.
809 Stocker, T.: Climate change 2013: the physical science basis: Working Group I contribution to the Fifth assessment
810 report of the Intergovernmental Panel on Climate Change, 2014.
811 Stolzenburg, D., Fischer, L., Vogel, A. L., Heinritzi, M., Schervish, M., Simon, M., Wagner, A. C., Dada, L.,
812 Ahonen, L. R., Amorim, A., Baccarini, A., Bauer, P. S., Baumgartner, B., Bergen, A., Bianchi, F., Breitenlechner,
813 M., Brilke, S., Buenrostro Mazon, S., Chen, D., Dias, A., Draper, D. C., Duplissy, J., El Haddad, I., Finkenzeller,
814 H., Frege, C., Fuchs, C., Garmash, O., Gordon, H., He, X., Helm, J., Hofbauer, V., Hoyle, C. R., Kim, C., Kirkby,
815 J., Kontkanen, J., Kürten, A., Lampilahti, J., Lawler, M., Lehtipalo, K., Leiminger, M., Mai, H., Mathot, S., Mentler,
816 B., Molteni, U., Nie, W., Nieminen, T., Nowak, J. B., Ojdanic, A., Onnela, A., Passananti, M., Petäjä, T., Quéléver,
817 L. L. J., Rissanen, M. P., Sarnela, N., Schallhart, S., Tauber, C., Tomé, A., Wagner, R., Wang, M., Weitz, L.,
818 Wimmer, D., Xiao, M., Yan, C., Ye, P., Zha, Q., Baltensperger, U., Curtius, J., Dommen, J., Flagan, R. C., Kulmala,
819 M., Smith, J. N., Worsnop, D. R., Hansel, A., Donahue, N. M., and Winkler, P. M.: Rapid growth of organic aerosol
820 nanoparticles over a wide tropospheric temperature range, Proceedings of the National Academy of Sciences, 115,
821 9122, 10.1073/pnas.1807604115, 2018.
822 Tan, Q., Ge, B., Xu, X., Gan, L., Yang, W., Chen, X., Pan, X., Wang, W., Li, J., and Wang, Z.: Increasing impacts
823 of the relative contributions of regional transport on air pollution in Beijing: Observational evidence, Environmental
824 Pollution, 292, 118407, https://doi.org/10.1016/j.envpol.2021.118407, 2022.
825 Teng, A. P., Crounse, J. D., and Wennberg, P. O.: Isoprene Peroxy Radical Dynamics, Journal of the American
826 Chemical Society, 139, 5367-5377, 10.1021/jacs.6b12838, 2017.
827 Tröstl, J., Chuang, W. K., Gordon, H., Heinritzi, M., Yan, C., Molteni, U., Ahlm, L., Frege, C., Bianchi, F., Wagner,
828 R., Simon, M., Lehtipalo, K., Williamson, C., Craven, J. S., Duplissy, J., Adamov, A., Almeida, J., Bernhammer,
829 A.-K., Breitenlechner, M., Brilke, S., Dias, A., Ehrhart, S., Flagan, R. C., Franchin, A., Fuchs, C., Guida, R., Gysel,

M., Hansel, A., Hoyle, C. R., Jokinen, T., Junninen, H., Kangasluoma, J., Keskinen, H., Kim, J., Krapf, M., Kürten, A., Laaksonen, A., Lawler, M., Leiminger, M., Mathot, S., Möhler, O., Nieminen, T., Onnela, A., Petäjä, T., Piel, F. M., Miettinen, P., Rissanen, M. P., Rondo, L., Sarnela, N., Schobesberger, S., Sengupta, K., Sipilä, M., Smith, J. N., Steiner, G., Tomè, A., Virtanen, A., Wagner, A. C., Weingartner, E., Wimmer, D., Winkler, P. M., Ye, P., Carslaw, K. S., Curtius, J., Dommen, J., Kirkby, J., Kulmala, M., Riipinen, I., Worsnop, D. R., Donahue, N. M., and Baltensperger, U.: The role of low-volatility organic compounds in initial particle growth in the atmosphere, Nature, 533, 527-531, 10.1038/nature18271, 2016.

Wagner, P., and Kuttler, W.: Biogenic and anthropogenic isoprene in the near-surface urban atmosphere — A case study in Essen, Germany, Science of The Total Environment, 475, 104-115, https://doi.org/10.1016/j.scitotenv.2013.12.026, 2014.

Wang, H., Lu, K., Guo, S., Wu, Z., Shang, D., Tan, Z., Wang, Y., Le Breton, M., Lou, S., Tang, M., Wu, Y., Zhu, W., Zheng, J., Zeng, L., Hallquist, M., Hu, M., and Zhang, Y.: Efficient N_2O_5 uptake and NO_3 oxidation in the outflow of urban Beijing, Atmos. Chem. Phys., 18, 9705-9721, 10.5194/acp-18-9705-2018, 2018a.

Wang, L., Liu, Z., Sun, Y., Ji, D., and Wang, Y.: Long-range transport and regional sources of PM2.5 in Beijing based on long-term observations from 2005 to 2010, Atmospheric Research, 157, 37-48, https://doi.org/10.1016/j.atmosres.2014.12.003, 2015.

Wang, S., Wu, R., Berndt, T., Ehn, M., and Wang, L.: Formation of Highly Oxidized Radicals and Multifunctional Products from the Atmospheric Oxidation of Alkylbenzenes, Environmental Science & Technology, 51, 8442-8449, 10.1021/acs.est.7b02374, 2017.

Wang, S., Riva, M., Yan, C., Ehn, M., and Wang, L.: Primary Formation of Highly Oxidized Multifunctional Products in the OH-Initiated Oxidation of Isoprene: A Combined Theoretical and Experimental Study, Environmental Science & Technology, 52, 12255-12264, 10.1021/acs.est.8b02783, 2018b.

Wang, Y., Hu, M., Wang, Y., Zheng, J., Shang, D., Yang, Y., Liu, Y., Li, X., Tang, R., Zhu, W., Du, Z., Wu, Y., Guo, S., Wu, Z., Lou, S., Hallquist, M., and Yu, J. Z.: The formation of nitro-aromatic compounds under high NO_x and anthropogenic VOC conditions in urban Beijing, China, Atmos. Chem. Phys., 19, 7649-7665, 10.5194/acp-19-7649-2019, 2019.

Wang, Z., Ehn, M., Rissanen, M. P., Garmash, O., Quéléver, L., Xing, L., Monge-Palacios, M., Rantala, P., Donahue, N. M., Berndt, T., and Sarathy, S. M.: Efficient alkane oxidation under combustion engine and atmospheric conditions, Communications Chemistry, 4, 18, 10.1038/s42004-020-00445-3, 2021.

Wu, R., Vereecken, L., Tsiligiannis, E., Kang, S., Albrecht, S. R., Hantschke, L., Zhao, D., Novelli, A., Fuchs, H., Tillmann, R., Hohaus, T., Carlsson, P. T. M., Shenolikar, J., Bernard, F., Crowley, J. N., Fry, J. L., Brownwood, B., Thornton, J. A., Brown, S. S., Kiendler-Scharr, A., Wahner, A., Hallquist, M., and Mentel, T. F.: Molecular composition and volatility of multi-generation products formed from isoprene oxidation by nitrate radical, Atmos. Chem. Phys., 21, 10799-10824, 10.5194/acp-21-10799-2021, 2021.

Xu, L., Møller, K. H., Crounse, J. D., Kjaergaard, H. G., and Wennberg, P. O.: New Insights into the Radical Chemistry and Product Distribution in the OH-Initiated Oxidation of Benzene, Environmental Science & Technology, 54, 13467-13477, 10.1021/acs.est.0c04780, 2020.

Xu, Z. N., Nie, W., Liu, Y. L., Sun, P., Huang, D. D., Yan, C., Krechmer, J., Ye, P. L., Xu, Z., Qi, X. M., Zhu, C. J., Li, Y. Y., Wang, T. Y., Wang, L., Huang, X., Tang, R. Z., Guo, S., Xiu, G. L., Fu, Q. Y., Worsnop, D., Chi, X. G., and Ding, A. J.: Multifunctional Products of Isoprene Oxidation in Polluted Atmosphere and Their Contribution to SOA, Geophysical Research Letters, 48, e2020GL089276, https://doi.org/10.1029/2020GL089276, 2021.

Yan, C., Nie, W., Äijälä, M., Rissanen, M. P., Canagaratna, M. R., Massoli, P., Junninen, H., Jokinen, T., Sarnela, N., Häme, S. A. K., Schobesberger, S., Canonaco, F., Yao, L., Prévôt, A. S. H., Petäjä, T., Kulmala, M., Sipilä, M., Worsnop, D. R., and Ehn, M.: Source characterization of highly oxidized multifunctional compounds in a boreal forest environment using positive matrix factorization, Atmos. Chem. Phys., 16, 12715-12731, 10.5194/acp-16-12715-2016, 2016.

Yan, C., Nie, W., Vogel, A. L., Dada, L., Lehtipalo, K., Stolzenburg, D., Wagner, R., Rissanen, M. P., Xiao, M., Ahonen, L., Fischer, L., Rose, C., Bianchi, F., Gordon, H., Simon, M., Heinritzi, M., Garmash, O., Roldin, P., Dias, A., Ye, P., Hofbauer, V., Amorim, A., Bauer, P. S., Bergen, A., Bernhammer, A. K., Breitenlechner, M., Brilke, S., Buchholz, A., Mazon, S. B., Canagaratna, M. R., Chen, X., Ding, A., Dommen, J., Draper, D. C., Duplissy, J., Frege, C., Heyn, C., Guida, R., Hakala, J., Heikkinen, L., Hoyle, C. R., Jokinen, T., Kangasluoma, J., Kirkby, J., Kontkanen, J., Kürten, A., Lawler, M. J., Mai, H., Mathot, S., Mauldin, R. L., Molteni, U., Nichman, L., Nieminen, T., Nowak, J., Ojdanic, A., Onnela, A., Pajunoja, A., Petäjä, T., Piel, F., Quéléver, L. L. J., Sarnela, N., Schallhart, S., Sengupta, K., Sipilä, M., Tomé, A., Tröstl, J., Väisänen, O., Wagner, A. C., Ylisirniö, A., Zha, Q., Baltensperger, U., Carslaw, K. S., Curtius, J., Flagan, R. C., Hansel, A., Riipinen, I., Smith, J. N., Virtanen, A., Winkler, P. M., Donahue, N. M., Kerminen, V. M., Kulmala, M., Ehn, M., and Worsnop, D. R.: Size-dependent influence of NOx on the growth rates of organic aerosol particles, Science Advances, 6, eaay4945, 10.1126/sciadv.aay4945, 2020.

Yan, C., Yin, R., Lu, Y., Dada, L., Yang, D., Fu, Y., Kontkanen, J., Deng, C., Garmash, O., Ruan, J., Baalbaki, R., Schervish, M., Cai, R., Bloss, M., Chan, T., Chen, T., Chen, Q., Chen, X., Chen, Y., Chu, B., Dällenbach, K., Foreback, B., He, X., Heikkinen, L., Jokinen, T., Junninen, H., Kangasluoma, J., Kokkonen, T., Kurppa, M., Lehtipalo, K., Li, H., Li, H., Li, X., Liu, Y., Ma, Q., Paasonen, P., Rantala, P., Pileci, R. E., Rusanen, A., Sarnela, N., Simonen, P., Wang, S., Wang, W., Wang, Y., Xue, M., Yang, G., Yao, L., Zhou, Y., Kujansuu, J., Petäjä, T., Nie, W., Ma, Y., Ge, M., He, H., Donahue, N. M., Worsnop, D. R., Veli-Matti, K., Wang, L., Liu, Y., Zheng, J., Kulmala, M., Jiang, J., and Bianchi, F.: The Synergistic Role of Sulfuric Acid, Bases, and Oxidized Organics Governing New-Particle Formation in Beijing, Geophysical Research Letters, 48, e2020GL091944, https://doi.org/10.1029/2020GL091944, 2021.

Ye, C., Yuan, B., Lin, Y., Wang, Z., Hu, W., Li, T., Chen, W., Wu, C., Wang, C., Huang, S., Qi, J., Wang, B., Wang, C., Song, W., Wang, X., Zheng, E., Krechmer, J. E., Ye, P., Zhang, Z., Wang, X., Worsnop, D. R., and Shao, M.: Chemical characterization of oxygenated organic compounds in gas-phase and particle-phase using iodide-CIMS with FIGAERO in urban air, Atmos. Chem. Phys. Discuss., 2020, 1-62, 10.5194/acp-2020-1187, 2020.

Zaytsev, A., Koss, A. R., Breitenlechner, M., Krechmer, J. E., Nihill, K. J., Lim, C. Y., Rowe, J. C., Cox, J. L., Moss, J., Roscioli, J. R., Canagaratna, M. R., Worsnop, D. R., Kroll, J. H., and Keutsch, F. N.: Mechanistic study of the formation of ring-retaining and ring-opening products from the oxidation of aromatic compounds under urban atmospheric conditions, Atmos. Chem. Phys., 19, 15117-15129, 10.5194/acp-19-15117-2019, 2019.

Zha, Q., Yan, C., Junninen, H., Riva, M., Sarnela, N., Aalto, J., Quéléver, L., Schallhart, S., Dada, L., Heikkinen, L., Peräkylä, O., Zou, J., Rose, C., Wang, Y., Mammarella, I., Katul, G., Vesala, T., Worsnop, D. R., Kulmala, M., Petäjä, T., Bianchi, F., and Ehn, M.: Vertical characterization of highly oxygenated molecules (HOMs) below and above a boreal forest canopy, Atmos. Chem. Phys., 18, 17437-17450, 10.5194/acp-18-17437-2018, 2018.

Zhang, H., Li, H., Zhang, Q., Zhang, Y., Zhang, W., Wang, X., Bi, F., Chai, F., Gao, J., Meng, L., Yang, T., Chen, Y., Cheng, Q., and Xia, F.: Atmospheric Volatile Organic Compounds in a Typical Urban Area of Beijing: Pollution Characterization, Health Risk Assessment and Source Apportionment, Atmosphere, 8, 10.3390/atmos8030061, 2017.

912 Zhang, H., Zhang, Y., Huang, Z., Acton, W. J. F., Wang, Z., Nemitz, E., Langford, B., Mullinger, N., Davison, B.,
913 Shi, Z., Liu, D., Song, W., Yang, W., Zeng, J., Wu, Z., Fu, P., Zhang, Q., and Wang, X.: Vertical profiles of biogenic
914 volatile organic compounds as observed online at a tower in Beijing, Journal of Environmental Sciences, 95, 33-42,
915 https://doi.org/10.1016/j.jes.2020.03.032, 2020.
916 Zhang, Q., Jimenez, J. L., Canagaratna, M. R., Allan, J. D., Coe, H., Ulbrich, I., Alfarra, M. R., Takami, A.,
917 Middlebrook, A. M., Sun, Y. L., Dzepina, K., Dunlea, E., Docherty, K., DeCarlo, P. F., Salcedo, D., Onasch, T.,
918 Jayne, J. T., Miyoshi, T., Shimono, A., Hatakeyama, S., Takegawa, N., Kondo, Y., Schneider, J., Drewnick, F.,
919 Borrmann, S., Weimer, S., Demerjian, K., Williams, P., Bower, K., Bahreini, R., Cottrell, L., Griffin, R. J.,
920 Rautiainen, J., Sun, J. Y., Zhang, Y. M., and Worsnop, D. R.: Ubiquity and dominance of oxygenated species in
921 organic aerosols in anthropogenically-influenced Northern Hemisphere midlatitudes, Geophysical Research Letters,
922 34, https://doi.org/10.1029/2007GL029979, 2007.
923 Zhang, Y.-Q., Ding, X., He, Q.-F., Wen, T.-X., Wang, J.-Q., Yang, K., Jiang, H., Cheng, Q., Liu, P., Wang, Z.-R.,
924 He, Y.-F., Hu, W.-W., Wang, Q.-Y., Xin, J.-Y., Wang, Y.-S., and Wang, X.-M.: Observational Insights into
925 Isoprene Secondary Organic Aerosol Formation through the Epoxide Pathway at Three Urban Sites from Northern
926 to Southern China, Environmental Science & Technology, 56, 4795-4805, 10.1021/acs.est.1c06974, 2022.
927 Zhang, Y., Peräkylä, O., Yan, C., Heikkinen, L., Äijälä, M., Daellenbach, K. R., Zha, Q., Riva, M., Garmash, O.,
928 Junninen, H., Paatero, P., Worsnop, D., and Ehn, M.: A novel approach for simple statistical analysis of high-
929 resolution mass spectra, Atmos. Meas. Tech., 12, 3761-3776, 10.5194/amt-12-3761-2019, 2019.
930 Zhao, Y., Thornton, J. A., and Pye, H. O. T.: Quantitative constraints on autoxidation and dimer formation from
931 direct probing of monoterpene-derived peroxy radical chemistry, Proceedings of the National Academy of Sciences,
932 115, 12142, 10.1073/pnas.1812147115, 2018.

933